Transpressional tectonics and Carboniferous magmatism in the Limousin, Massif Central, France:structural and 40Ar/39Ar investigations.

Aude Gébelin, Maurice Brunel, Patrick Monié, Michel Faure, Nicolas Arnaud

▶ **To cite this version:**

Aude Gébelin, Maurice Brunel, Patrick Monié, Michel Faure, Nicolas Arnaud. Transpressional tectonics and Carboniferous magmatism in the Limousin, Massif Central, France:structural and 40Ar/39Ar investigations.. Tectonics, 2007, 26 (2), pp.TC2008. 10.1029/2005TC001822 . hal-00104212

HAL Id: hal-00104212
https://insu.hal.science/hal-00104212

Submitted on 2 Nov 2010

HAL is a multi-disciplinary open access archive for the deposit and dissemination of scientific research documents, whether they are published or not. The documents may come from teaching and research institutions in France or abroad, or from public or private research centers.

L'archive ouverte pluridisciplinaire **HAL**, est destinée au dépôt et à la diffusion de documents scientifiques de niveau recherche, publiés ou non, émanant des établissements d'enseignement et de recherche français ou étrangers, des laboratoires publics ou privés.

Click Here for Full Article

Transpressional tectonics and Carboniferous magmatism in the Limousin, Massif Central, France: Structural and $^{40}Ar/^{39}Ar$ investigations

Aude Gébelin,[1,2] Maurice Brunel,[1] Patrick Monié,[1] Michel Faure,[3] and Nicolas Arnaud[1]

Received 1 April 2005; revised 8 August 2006; accepted 14 September 2006; published 27 March 2007.

[1] New structural, microstructural, and $^{40}Ar/^{39}Ar$ data from the NW Massif Central (France) provide additional constraints on the timing and tectonic setting of late Variscan granite magmatism. Previous studies had emphasized the role of late orogenic extension in the emplacement of granite plutons in the Limousin region. In contrast, the new data set is consistent with syntectonic emplacement of magma in a dextral simple shear active from 350 to 300 Ma in a transpressional regime. As an alternative hypothesis to late orogenic extension, we propose that magmas migrated into tensional bridges between active P shears associated with a lithospheric shear zone comparable to a pop-up structure. The Galician region, in the western end of the Ibero-Armorican tectonic arc, exhibits major left-lateral ductile shear zones which can be interpreted as conjugate structures to the Limousin and Armorican shear zones. **Citation:** Gébelin, A., M. Brunel, P. Monié, M. Faure, and N. Arnaud (2007), Transpressional tectonics and Carboniferous magmatism in the Limousin, Massif Central, France: Structural and $^{40}Ar/^{39}Ar$ investigations, *Tectonics*, *26*, TC2008, doi:10.1029/2005TC001822.

1. Introduction

[2] Many studies have shown that melts have an influence on the rheology and deformation of the continental crust [e.g., *Davidson et al.*, 1994]. A number of examples show a close spatial and temporal relationship between magmas and crustal ductile shear zones [*Hutton and Reavy*, 1992; *Davidson et al.*, 1992; *Tikoff and Teyssier*, 1992; *Neves et al.*, 1996; *Tikoff and de Saint Blanquat*, 1997]. Field observations lead to the following questions: does lithospheric deformation trigger magma formation and ascent? Does magma rheology have an impact on the location of the crustal deformation? The Variscan granite plutons in the Limousin region, western Europe, constitute a remarkable natural laboratory to debate these questions.

[3] The Variscan Belt of western Europe was built between 500 and 250 Ma from the convergence and collision of two main continents, Laurentia-Baltica to the northwest and Gondwana to the southeast [e.g., *Matte*, 1991]. Postcollisional intracontinental tectonothermal events extended over a time span of 100 Myr, between 380 and 280 Ma [*Matte*, 1991]. The Limousin area, in the northwest part of the Massif Central (France), first experienced crustal shortening and thickening [*Matte*, 1986], followed by extension and crustal thinning [*Van den Driesche and Brun*, 1989; *Faure et al.*, 1990; *Burg et al.*, 1990; *Faure*, 1995]. It is characterized by voluminous two-mica leucogranites resulting from partial melting of the Variscan crustal basement [e.g., *Cuney et al.*, 1990]. These intrusions are spatially associated with normal faults and major synmagmatic strike-slip shear zones that merge to the northwest with the South Armorican Shear Zone (SASZ). Previous studies emphasized the role of Carboniferous late orogenic extension and normal faults in the emplacement of Limousin granite plutons [*Faure*, 1989; *Faure and Pons*, 1991; *Faure*, 1995]. However, new field evidences suggest that strike-slip faults were also closely associated with magma genesis. What are the relationships then between strike-slip and normal faulting contemporaneous with granites emplacement?

[4] The purpose of this paper is to describe the structures and microstructures of rocks affected by ductile strike-slip shearing in the Limousin area, and to present new $^{40}Ar/^{39}Ar$ geochronological data. These data, collected from the core and border of granitic plutons and from wall rocks, show that strike-slip faulting started around 350 Ma and ended around 300 Ma. The structural study was performed in order to better understand: (1) the deformation mechanisms that prevailed during cooling of the granites; (2) the relationships between the tectonic setting and late Variscan granite emplacement; and (3) the mechanisms of magma migration and emplacement.

[5] After a thorough structural characterization and argon thermochronology investigations on the Limousin area, comparisons are made with other parts of the Armorican Massif. The new results are then synthesized in a discussion in which we propose that granitic magmatism took place in a transpressional context where the magmas were emplaced into tensional bridges between active P shears. Some of the implications of this new interpretation are discussed in the framework of the French Massif Central. Finally, the new

[1]Laboratoire Dynamique de la Lithosphère, UMR 5573, Université Montpellier II, Montpellier, France.
[2]Now at Mining Business Unit, AREVA NC, Vélizy, France.
[3]Institut des Sciences de la Terre d'Orléans, UMR 6113, Université d'Orléans, Orléans, France.

Copyright 2007 by the American Geophysical Union.
0278-7407/07/2005TC001822$12.00

results are integrated in a general geodynamic model at the scale of the Limousin and Armorican massifs.

2. Geological Setting and Previous Work

2.1. Massif Central (France) in the Variscan Belt

[6] The West European Variscan Belt formed as a result of a Himalaya-type continental collision between the Laurentia-Baltica and Gondwana lithospheric plates [e.g., *Matte*, 1991]. In the French Massif Central, the Variscan orogenic events range from Late Silurian–Early Devonian, i.e., 440–400 Ma, which is a period of high-pressure (HP) metamorphism [*Ledru et al.*, 1989; *Santallier et al.*, 1994; *Faure et al.*, 1997; *Matte et al.*, 1998], up to Late Carboniferous–Early Permian, i.e., 300 Ma which is the deposition time of the late orogenic sediments.

[7] Eclogites are associated with felsic and mafic HP granulites [*Nicollet and Leyreloup*, 1978; *Pin and Vielzeuf*, 1983] and with spinel and/or garnet lherzolites [*Gardien et al.*, 1988; *Gardien*, 1990]. The P-T conditions of the eclogite facies metamorphism are estimated to 13–20 kbar and 650–750°C [*Mercier et al.*, 1991]. The coesite-bearing eclogites of eastern Massif Central [*Lardeaux et al.*, 2001] were brought to shallow crustal levels during continental collision. Eclogite exhumation (~60 km of uplift) took place in a transpressive regime [*Lardeaux et al.*, 2001].

[8] The Middle Devonian to Early Carboniferous recorded continental collision and nappe stacking. Two gneissic units are distinguished in most parts of Massif Central [*Burg et al.*, 1984; *Santallier et al.*, 1988, 1994; *Ledru et al.*, 1989, 1994a; *Lardeaux et al.*, 2001]. The upper gneiss unit (UGU) contains HP metamorphic assemblages and is characterized, at its base, by a bimodal association, the so-called ''leptyno-amphibolite'' group. The UGU rests upon a frequently anatectic lower gneiss unit (LGU) which lacks HP metamorphic assemblages (Figure 1). However, the presence of synkinematic cordierite in the anatectic paragneisses of the LGU can be related to the isothermal decompression of the HP metamorphic assemblages (Figure 1) [*Mercier et al.*, 1992; *Santallier et al.*, 1994], under medium-pressure and high-temperature conditions (5–6 kbar, 760–780°C [*Le Breton and Thompson*, 1988]). These paragneisses yielded Rb/Sr whole rock isochrons of 375 ± 6 Ma [*Duthou*, 1977] and 384 ± 16 Ma [*Duthou et al.*, 1994]. Amphibolites of the Aigurande plateau (Figure 1) have an age of 389 ± 8 Ma ($^{40}Ar/^{39}Ar$ method [*Boutin and Montigny*, 1993]). Both UGU and LGU overlie a parautochthon unit of Paleozoic micaschists with minor orthogneiss [*Ledru et al.*, 1994b].

[9] The Late Carboniferous period is characterized by postorogenic extension [*Ménard and Molnar*, 1988; *Van Den Driesche and Brun*, 1991; *Faure*, 1995]. This stage is also marked by intramountainous coal-bearing basins that seal the end of the Variscan orogeny. These last events are contemporaneous with granulitic metamorphism in the lower crust [*Pin and Vielzeuf*, 1983; *Costa and Rey*, 1995].

2.2. Limousin Region

[10] The Limousin region, in the northwest of Massif Central, is a key area to understand Variscan tectonic and magmatic processes because of the voluminous granitic magmatism and its association with strike-slip shear zones. This region is overlain to the west by the ''Seuil du Poitou'' Mesozoic series and bounded to the east by the Stephanian ''Sillon Houiller'' sinistral strike-slip fault (Figure 1).

[11] The Limousin region, hosts two granite types: the biotite ± hornblende ± cordierite-bearing granites (Guéret type), and the two-mica leucogranites [e.g., *Scaillet et al.*, 1996a, 1996b]. The Guéret-type granites were emplaced in a transpressive setting [*Cuney et al.*, 2001] between 356 and 349 ± 5 Ma (U–Pb zircon age) [*Bertrand et al.*, 2001], at a depth of 14 ± 2 km [*Freiberger et al.*, 2001]. These granites are thought to be derived from the interface between metasedimentary and mafic igneous lower crust [*Downes and Duthou*, 1988; *Shaw*, 1991]. The Guéret Massif (Figure 1), emplaced at 356 ± 10 Ma (Rb/Sr on whole rocks [*Berthier et al.*, 1979]), hosts not only Guéret-type granites but also cordierite-bearing anatectic paragneisses. The unconformity of the ''Visean Tufs Anthracifères'' formation [*Faure et al.*, 2002] with the Guéret granite indicates that the granite was exposed at the surface at 335 Ma. The Guéret massif is fault bounded (Figure 1) [*Grolier and Letourneur*, 1968; *Lerouge*, 1988] and is interpreted as an extensional allochton shifted to the south-east in Namurian-Westphalian times [*Faure and Pons*, 1991; *Faure*, 1995]. The granite has subhorizontal NW-SE magnetic foliations and magnetic lineations [*Jover*, 1986]. A recent gravity study has modeled the Guéret granite as a laccolith, less than a few hundred meters in thickness [*Gébelin et al.*, 2006]. These gravity results did not identify the feeder zones nor the chamber from which the granitic magmas originated.

[12] The two-mica leucogranites were emplaced after the Guéret granites, between 340 and 280 Ma [*Duthou et al.*, 1984; *Gébelin*, 2004]. Geochemical data suggest that they derived from partial melting of a crustal protolith with no mantle component [*Vidal et al.*, 1984; *Turpin et al.*, 1990; *Shaw*, 1991]. These massifs are separated by large E-W to NW-SE striking mylonitic shear zones and subsequently cut by N-S normal shear zones (Figure 1). They were initially interpreted as diapirs emplaced in the core of gneiss-micaschist domes [*Grolier*, 1971; *Lameyre*, 1982, 1984], then as syntectonic sheets emplaced during northwest trending ductile shear [*Mollier and Bouchez*, 1982; *Bouchez and Jover*, 1986; *Jover and Bouchez*, 1986]. More recently, *Faure and Pons* [1991] and *Faure* [1995] have proposed a late Visean to Namurian emplacement, during crustal thinning contemporaneously with normal faulting in response to a NW-SE extension. Recent investigations emphasize the laccolithic geometry (<4 km thick) of the synmagmatic two-mica leucogranites [*Gébelin et al.*, 2004, 2006]. The proposed model of emplacement includes magma ascent along vertical strike-slip shear zones followed by lateral migration along the preexisting horizontal foliation. The main leucogranitic massifs of this region (Figure 1) are briefly described in the following.

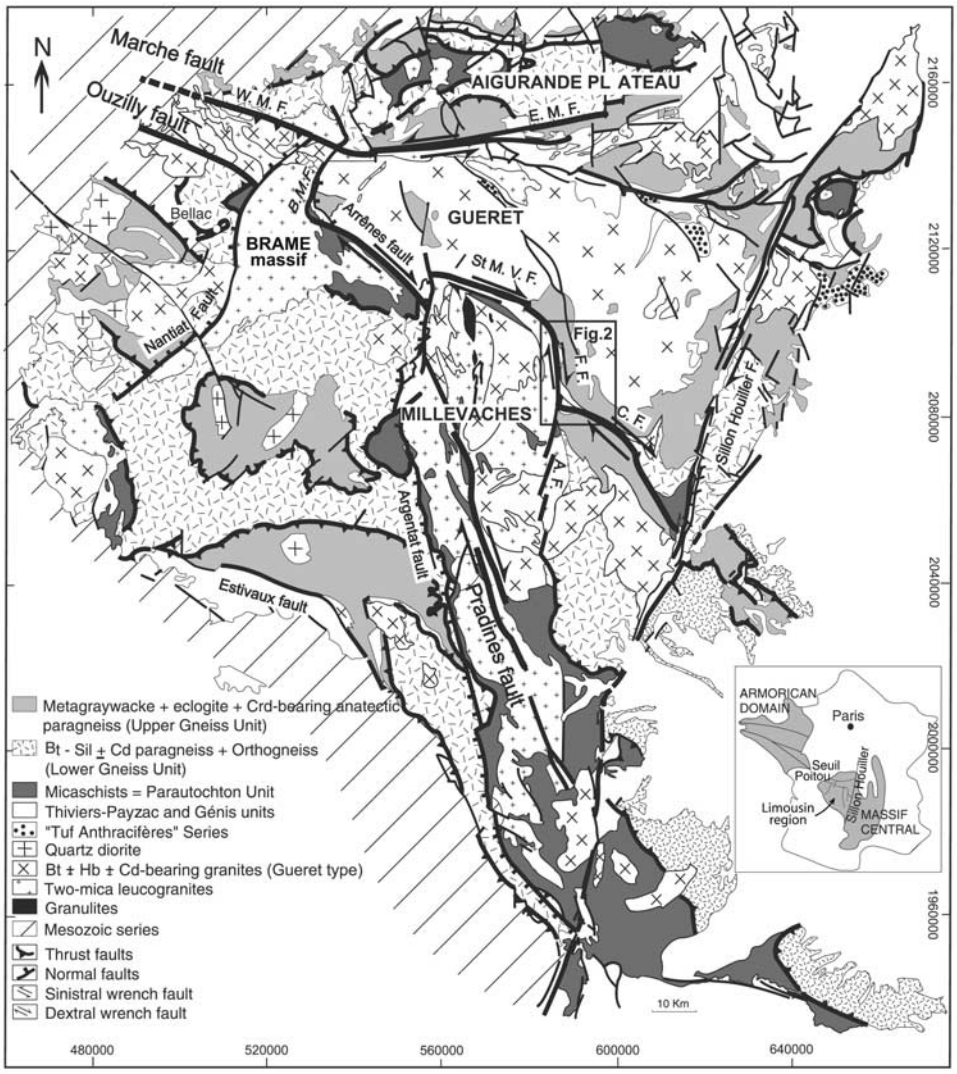

Figure 1. Simplified geological map of the northwestern part of the French Massif Central. BMF, Bussières-Madeleine fault; WMF, West Marche fault; EMF, East Marche fault; St M. V. F., St Michel de Veisse fault; FF, Felletin fault; CF, Courtine fault; AF, Ambrugeat fault.

[13] The Aigurande plateau, an antiformal stack of pre-Visean nappes, located in the northern part of the Limousin (Figure 1) [*Quenardel and Rolin*, 1984], hosts two-mica leucogranites. Granite emplacement is considered syntectonic [*Rolin and Quenardel*, 1982; *Launeau et al.*, 1988] and constrained by two Rb/Sr whole rock age at 312 ± 20 Ma and 312 ± 6 Ma [*Petitpierre and Duthou*, 1980; *Rolin et al.*, 1982]. These granitic bodies have been modeled as 2-km-thick plutons rooted in the Marche fault plane to the south (Figure 1) [*Dumas et al.*, 1990; *Gébelin et al.*, 2006].

[14] The Marche two-mica leucogranites are located along the E-W to NW-SE Marche fault that separates the Aigurande plateau to the north from the Guéret massif to the south (Figure 1). These granites, which have recorded a synmagmatic ductile deformation during the sinistral wrench fault activity [*Choukroune et al.*, 1983; *Dumas et al.*, 1990], are related to a high-gravity negative anomaly [*Gébelin et al.*, 2006], coeval with the interpretation of the Marche fault as a feeding zone.

[15] The Brâme two-mica leucogranites, bounded by normal faults [*Mollier and Bouchez*, 1982; *Faure*, 1989, 1995] (Figure 1), was emplaced syntectonically 324 ± 4 Ma (U-Pb on zircon [*Holliger et al.*, 1986]), at depth of 10.5 ± 1 km [*Scaillet et al.*, 1996b]. K-Ar results are consistent with progressive exhumation along detachment faults and cooling from about 320 to 305 Ma including a rapid exhumation stage (1.5 mm/yr) at circa 305 Ma [*Scaillet et al.*, 1996a]. This massif displays a large aspect ratio, a relatively small thickness of about 2 to 4 km and an overall near-horizontal foliation [*Audrain et al.*, 1989; *Gébelin et al.*, 2006].

[16] The Millevaches massif, in the center of the Limousin (Figure 1) trends N-S and consists of several biotite ± cordierite-bearing porphyritic granites and two-mica leucogranites hosted in micaschists forming elongated N-S or

NW-SE trending units. This massif is fault bounded to the west, by the brittle-ductile Argentat normal fault [*Lameyre*, 1984; *Ledru and Autran*, 1987; *Mattauer et al.*, 1988] and to the north and the east by dextral strike-slip faults (Figure 1). The Pradines shear zone is a 5-km-wide, N-S striking dextral strike-slip fault that cuts the Millevaches massif in its center (Figure 1). The Millevaches massif is a representative example of Limousin syntectonic granites that shows a sigmoidal map pattern of magnetic foliations and lineations consistent with right-lateral shear (Figure 1) [*Gébelin et al.*, 2004, 2006]. Magnetic foliations are steep in the center of the Pradines shear zone and gradually become subhorizontal outside. The three-dimensional (3-D) shape at depth of this granite body, investigated using gravimetric data inversion [*Gébelin et al.*, 2004, 2006], is that of a laccolith (<4 km thick). The proposed model of emplacement includes magma ascent along the vertical strike-slip Pradines fault which channeled magmas from depth to their middle crust emplacement level followed by lateral migration along the preexisting horizontal foliation [*Gébelin et al.*, 2004, 2006].

3. Structural Analysis

[17] The Limousin region is characterized by three major strike-slip ductile faults systems cut by normal faults (Figure 1). The E-W Marche fault system includes the West and East Marche faults (WMF and EMF). The NW-SE Ouzilly fault system includes the Arrênes, St Michel de Veisse, Felletin and Courtine faults. The NNW-SSE Pradines fault, probably a branch of the Ouzilly fault, crosscuts the Millevaches Massif.

[18] To avoid repetition in the description, we usually use the term ''fault'' as shear zone in the large sense of the word, meaning that like a fault, a shear zone accumulates relative displacement of rock bodies, but unlike a fault, displacement in a ductile shear zone occurs by ductile deformation mechanisms and no throughgoing fracture is formed.

3.1. Marche Fault System

[19] In the western portion of this fault system (Figure 1), the Marche fault deforms the two-mica leucogranites and the LGU. The foliation strikes N120° and dips 80° SW, and the mineral lineation has a pitch of 50° toward the West Micafish microstructures and σ-type pressure shadows indicate a northeastward sinistral reverse sense of shear. In the eastern portion of the shear zone (EMF, Figure 1), the foliation strikes N100° with a vertical dip, and the mineral lineation is horizontal. Our observations of macroscopic shear sense criteria, in agreement with *Choukroune et al.* [1983], support a ductile sinistral shear along the Marche shear zone.

3.2. Ouzilly Fault System

[20] The Ouzilly fault system is cut off by the Brâme massif and the Millevaches Massif as well as a number of normal faults (Figure 1). It is a ~1-km-wide dextral strike-slip fault system that deforms biotite ± cordierite-bearing granites (Guéret type), two-mica leucogranites and biotite-sillimanite ± cordierite gneisses of the LGU.

[21] The Ouzilly fault system bounds the northern edge of the Millevaches Massif. The foliation in the two-mica leucogranites and in the LGU gneisses strikes E-W to NW-SE and dips between 55° and 85°N, while the mineral lineation plunges shallowly. Kinematic criteria associated with the subhorizontal lineation (asymmetric plagioclase augens, boudinage and mica fish structures) indicate a dextral sense of shear. To the SE, the subvertical foliation gradually follows the edge of the Millevaches pluton: from E-W to NW-SE striking along the Saint Michel de Veisse fault, it becomes N-S striking along the Felletin fault (FF, Figure 1). At large strain and by simple shear, particles in suspension flow tend to get a shape-preferred orientation parallel to the flow plane, and heterogeneous flow, with flow partitioning, produces magmatic structures as sinistral and dextral magmatic shear bands in two-mica leucogranites. Most of the foliations in the margins of the Millevaches two-mica leucogranites strike NW-SE to NNW-SSE and dip between 60° and 80° NE (NW corner of Figure 2). Mineral lineations have similar orientations, while having shallow plunges. Magnetic fabrics, deduced from anisotropy of magnetic susceptibility measurements, confirm these field observations [*Gébelin et al.*, 2006].

[22] Along the eastern edge of the Millevaches Massif, the Ouzilly shear zone deforms the two-mica leucogranites that have recorded two deformation events. The first event produced a near vertical N-S foliation and a lineation gently plunging (<30°) to the south (Figure 2, zone 2, inserts F1 and a). Shear bands indicate a dextral sense of shear. Sinistral strike-slip movement in the Millevaches mylonitic leucogranites can be observed to the west and northwest of Felletin (see location on Figure 2). The second deformation event produced southwest directed reverse faulting. The associated foliation strikes NW-SE and dips gently (<30°) to the NE (Figure 2, zone 1, insert b). The lineation is oriented NE-SW and is associated with shear bands indicating a sinistral sense of shear (Figure 2, zone 1, insert b). Both dextral strike-slip faults and reverse faults can be observed within the same granite. The first and second lineations are defined by the orientation of mica wrapped around well-preserved feldspar porphyroclasts, and by deformed quartz grains (see auxiliary material Text S1, section 1).[1]

[23] The Ouzilly shear zone also deforms cordierite-bearing anatectic paragneisses, biotite-bearing granites (Guéret type) and biotite-sillimanite ± cordierite gneisses (LGU). North of the shear zone, the foliation in the gneisses and granites is orientated N310–N340 and dips between 20° and 85° NE from west to east (Figure 2, zone 1, insert F1). The foliation in the gneisses is compatible with the near horizontal S2 foliation in the two-mica leucogranites. The foliation in the biotite-bearing granites strikes N330° and dips 50° to NE and becomes subvertical near the anatectic paragneiss (Figure 2, zone 1). The lineation in the gneisses and the granites plunges gently (30°) to the north (Figure 2, zone 1, insert L1). Shear bands, particularly in the ultra-

[1] Auxiliary materials are available in the HTML. doi:10.1029/2005TC001822.

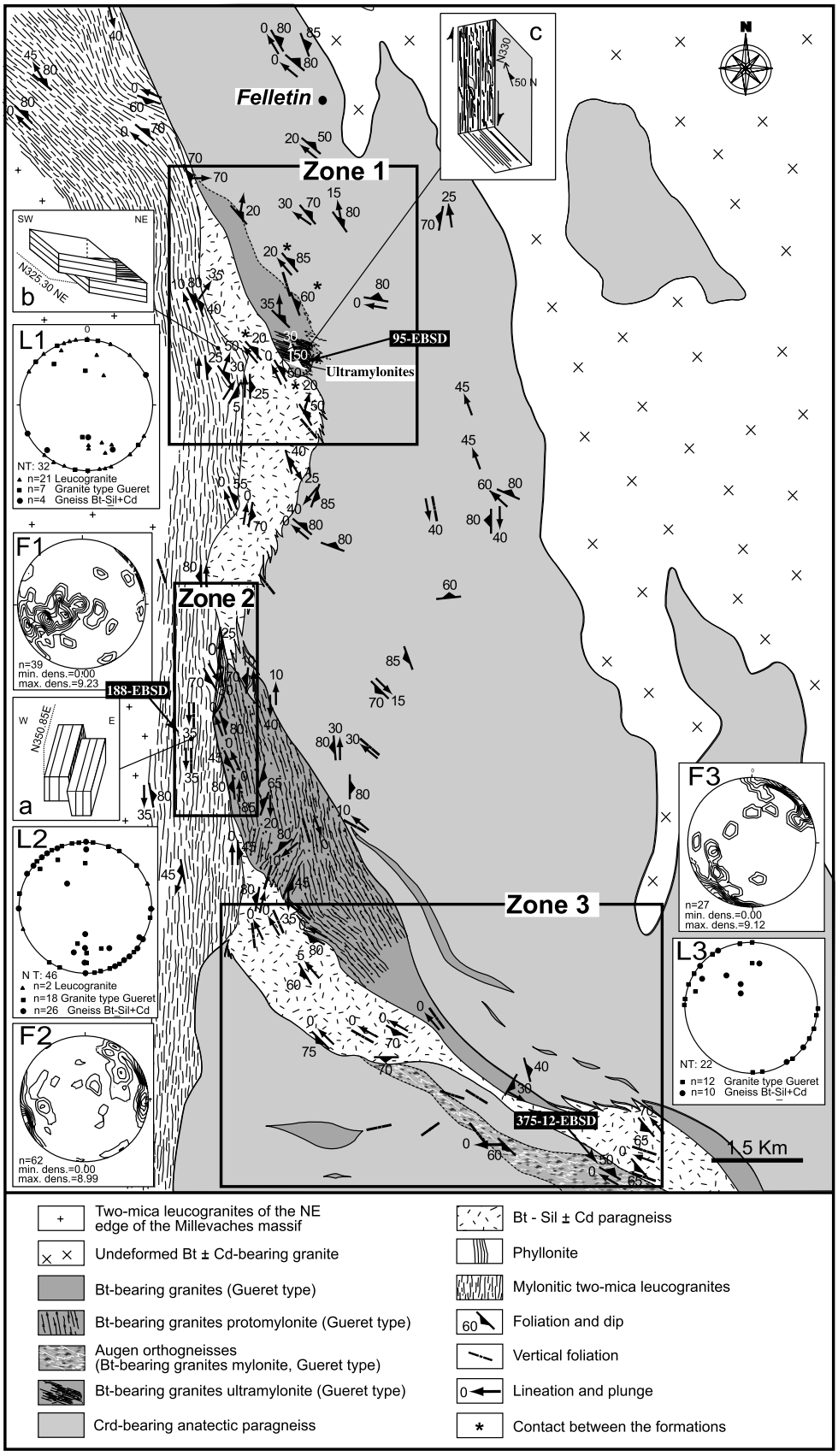

Figure 2. Geological map of Felletin–La Courtine shear zone.

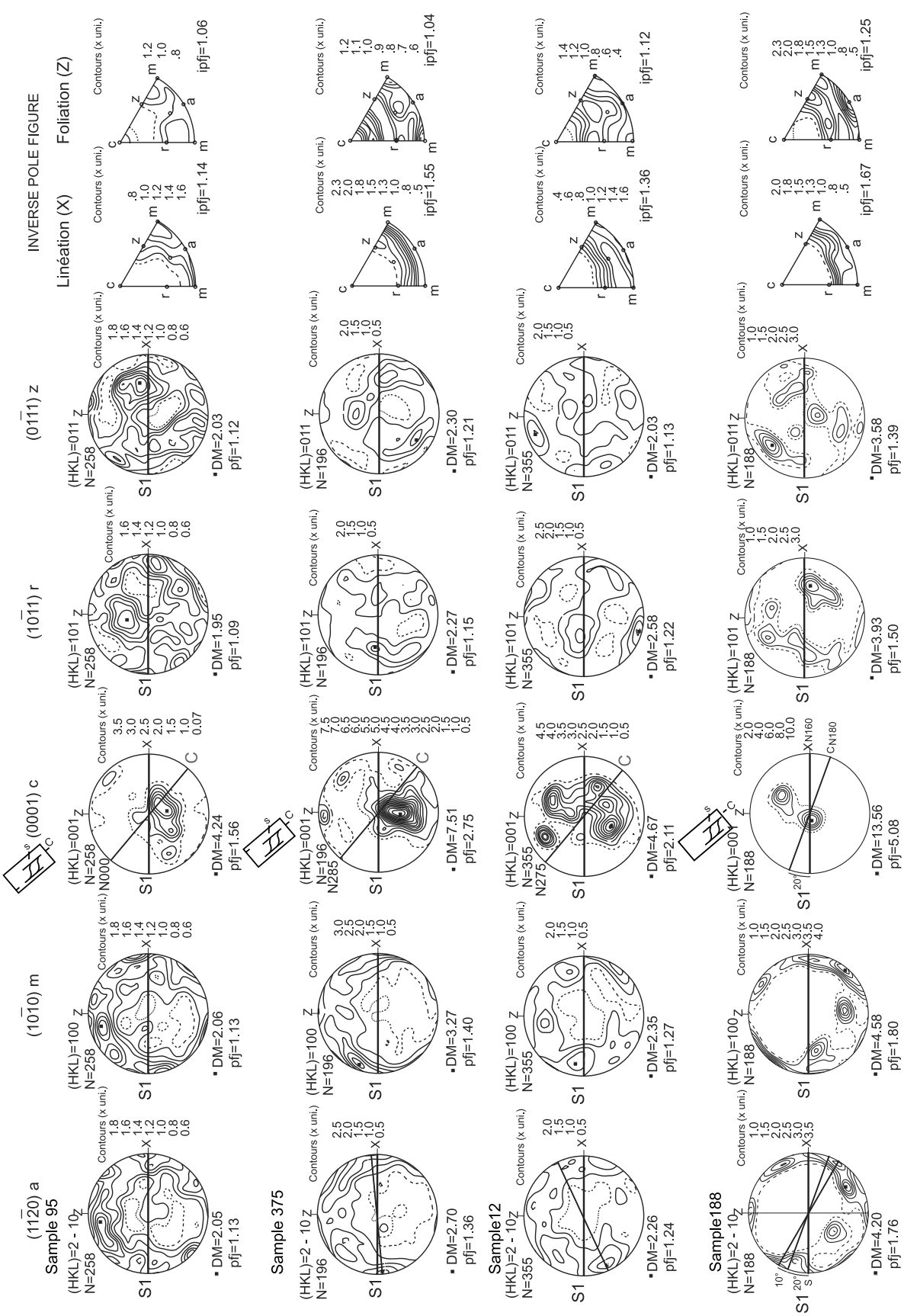

Figure 3. Quartz LPO measured using the EBSD technique. Equal-area projection, lower hemisphere. Foliation (XY plane) is vertical, and lineation (X) is horizontal in this plane. N, number of measurements. DM, maximum density.

mylonites of the biotite-bearing granites, indicate a top to the south sense of shear (sample 95, see ES, Figure 3). Southward, the shear zone moves away from the Millevaches two-mica leucogranites and from a N-S trending direction (Figure 2, zone 2, insert F2), the foliation gradually strikes NW-SE (Figure 2, zone 3, insert F3). Between zone 2 and zone 3 all foliations become near vertical (Figure 2, F2 and F3). Lineations are nearly horizontal with a plunge that rarely exceeds 25° to the southeast (Figure 2, inserts L2 and L3). Shear sense criteria indicate a dextral strike-slip movement.

[24] To the eastern end of the Ouzilly fault system, the LGU gneisses and biotite-bearing granites form lenses parallel to the general trend of the shear zone (Figure 2, zone 3). The foliation planes strike N300 and dip 55° to 80° SW (Figure 2, zone 3, insert F3). The lineations have a shallow plunge between 0° and 20° (Figure 2, zone 3, insert L3). Biotite-bearing granite outcrops in the NW-SE section show large shear bands that indicate a dextral sense of shear (samples 375, see auxiliary material Figure S1h). Feldspars have asymmetric pressure shadows containing small quartz and plagioclase grains (see auxiliary material Figure S2a).

3.3. Pradines Fault

[25] Within the fault, both the granite and micaschist display a foliation which strikes NNW-SSE, and dips steeply (>55°), with a subhorizontal lineation. The two-mica leucogranites show typical biotite-muscovite C-S mylonitic structures, characteristic of a dextral sense of shear (see Figures S1d and S1e). During the Pradines dextral strike-slip fault movement, micaschists underwent lit-par-lit partial melting (see Figure S2a) giving rise to lit-par-lit gneisses formed by sequential injection of granitic magma along the foliation planes of micaschists.

4. Quartz Preferred Orientation Analysis by Electron Backscattered Diffraction (Method and Analytical Details in Appendix A)

[26] Four representative samples of mylonitic granite from the Felletin–La Courtine ductile shear zones have been studied using the EBSD technique. The first rock (sample 95, see location on Figure 2, zone 1, and Figure S1f), sampled in the N-S striking section of the shear zone, consists of ultramylonitic biotite-bearing granites (see Text S1, section 2). The ultramylonite foliation strikes N330, dips 50° NE, and bears an N-S mineral lineation (Figure 2, zone 1). C-S microstructures indicate a top-to-south reverse sense of shear (see Figure S1f). Quartz grains concentrated in pure quartz layers are elongated at an angle of 35° with C planes (see Figure S1g). The quartz c axes fabric is of girdle type and contains a marked concentration of C axes parallel to the *Y axis* of the finite strain ellipsoid (Figure 3). This is compatible with plastic deformation by dominantly ⟨a⟩ prismatic glide, which occurs between 400°C and 700°C [*Tullis et al.*, 1973; *Mainprice and Paterson*, 1984]. The quartz c axes pole shows a small obliquity with respect to Y (Figure 3).

[27] Samples 12 and 375 (see Figure S1h) correspond to mylonites of biotite-bearing granites. They are located within the NW-SE striking section of the shear zone (Figure 2, zone 3). The foliation planes are subvertical and strike E-W, and the lineation is subhorizontal (Figure 2, zone 3). These samples experienced less intense deformation than the sample 95. The lineation is defined by the quartz grain shape orientation. The quartz c axes of sample 12 (Figure 3) are interpreted to result from preferential activation of prismatic ⟨a⟩ and rhombohedral glide systems. The a and m axis maxima make an angle of 20°–25° with the lineation (X). The r axis maximum has a bimodal distribution in the XZ plane at right angle with the foliation. The inverse pole figures (Figure 3) show the importance of the r plane and its direct relationships with the foliation and the lineation. For temperatures close to those developed during syntectonic granite crystallization, *Kruhl and Peternell* [2002] showed that quartz slip systems involve rhombhedral planes. The quartz c axes pattern of sample 375 shows a dominant maximum closer to the center and characterizes a dominant ⟨a⟩ prismatic glide (Figure 3). Another lower ponderated maximum develops in the XZ plane (Figure 3).

[28] Sample 188 is from the mylonitic two-mica leucogranites forming the NE edge of the Millevaches massif (Figure 2, zone 2). As seen previously, they present a N-S subvertical foliation and the lineation plunges shallowly with a N-S trend (Figure 2, zone 2). C-S relationships indicate dextral strike-slip movement (see Figure S1c). Quartz ribbons form microdextral shear bands and present a maximum grain shape orientation of around 40° with ribbon boundaries (see Figure S1c).

[29] The quartz c axes are clustered in the dominant maximum in the center (Y) of the pole figure (Figure 3). Another maximum develops at 40° from Y. The quartz a axis maximum is consistent with a dextral shear in agreement with field and microstructural observations (see Figure S1c).

[30] Such quartz fabric was acquired during the cooling of the biotite granite (Guéret type) and two-mica leucogranite. Thus the Ouzilly shear zone was already active at around 350 Ma or just after 350 Ma, i.e., the emplacement age of the Guéret-type granites [*Berthier et al.*, 1979].

5. The $^{40}Ar/^{39}Ar$ Results

[31] About 20 samples were collected along the Limousin ductile shear zones and in the leucogranitic massifs. (See analytical procedure in Appendix A and location of samples in Table 1.) In this study, different techniques of argon extraction were used. Bulk mineral samples (~10 mg) have been degassed using a classical step heating procedure in a double vacuum staudacher-type furnace. Step heating and spot fusion experiments were also performed on single grains with a continuous laser probe. In addition, in situ laser probe analyses have been conducted on polished thin rock sections, 10 mm × 10 mm and 1 mm thick. The combination of these different techniques has the advantage of giving important information on argon behavior during mylonitization and cooling of the various types of rocks.

Table 1. Sample Locations[a]

Sample	Lithology	Assemblages	Localization	C.L.II-X	C.L.II-Y
334	mylonitic two-mica leucogranite	Kfs,Pl,Qtz, Bt,Ms	West Marche fault-St Sulpice-les-Feuilles	519	2149.7
284c/284e	mylonitic two-mica leucogranite	Kfs,Pl,Qtz, Bt,Ms	East Marche fault-Dun-le-Palestel	548.6	2142.8
331	biotite-sillimanite ± cordierite gneiss	Qtz, Pl, Kfs, Bt, Ms, Sil	north of Marche fault-Marseuil	559.4	2145.7
246	mylonitic two-mica leucogranite	Kfs,Pl,Qtz, Bt,Ms	St Michel-de-Veisse fault-Pontarion	561	2113.8
241	biotite-sillimanite ± cordierite gneiss	Qtz, Pl, Kfs, Bt, Ms, Sil, Crd	St Michel-de-Veisse fault-St Hilaire-le-Château	565.5	2109.2
6	undeformed leucogranite	Kfs,Pl,Qtz, Bt,Ms	Millevaches massif-St Quentin-la-Chabanne	583.9	2093.85
524	mylonitic two-mica leucogranite	Kfs,Pl,Qtz, Bt,Ms	St Michel-de-Veisse fault-St Michel-de-Veisse	574.4	2107.7
3	mylonitic two-mica leucogranite	Kfs,Pl,Qtz, Bt,Ms	Felletin-La Courtine fault-west of Felletin	584.55	2098.15
265	mylonitic two-mica leucogranite	Kfs,Pl,Qtz, Bt,Ms	Felletin-La Courtine fault-St Quentin-la-Chabanne	585.9	2093.65
40	biotite-sillimanite ± cordierite gneiss	Qtz, Pl, Kfs, Bt, Ms, Sil, Crd	Felletin-La Courtine fault-Masd'Artige	435.6	2084
347	biotite-sillimanite ± cordierite gneiss	Qtz, Pl, Kfs, Bt, Ms, Sil, Crd	Felletin-La Courtine fault-Confolent-Port-Dieu	614.2	2060.55
356	mylonitic two-mica leucogranite	Kfs,Pl,Qtz, Bt,Ms	Pradines fault-Sarran	001°56′47″01	45°24′05″
404	granulite	Qtz, Pl, Kfs, Bt, Sil, Crd, Grt,sp	Pradines fault-St Pierre-Bellevue	565.1	2103.3

[a]C.L.II-X, X - II Lambert coordinates; C.L.II-Y, Y - II Lambert coordinates; Kfs, K-feldspar; Pl, plagioclase; Qtz, quartz; Bt, biotite; Ms, muscovite; Sil, sillimanite; Crd, cordierite; Grt, garnet; sp, spinelle.

For example, in mylonitic rocks, different generations of mica coexist, which developed at the time of granite emplacement and during subsequent shearing. In the most deformed samples, only the ultramylonitic facies shear bands of tiny secondary mica are present. Therefore the comparison of results from such rocks has the potential to give us age constraints on the cooling of the various granites, on their deformation and subsequent cooling, on the scale of argon migration during mylonitization, on the eventual presence of excess argon, and on the role of recrystallization as a factor in argon resetting.

5.1. Marche Fault and Surrounding Rocks

[32] Sample 334 is a mylonitic two-mica leucogranite from the west Marche fault. Using a bulk sample step-heating procedure, muscovite from this sample gives a plateau age (Figure 4a and Table 2) of 324.9 ± 3.0 Ma for 60% of the ^{39}Ar released, and an intercept age of 326.9 ± 3.0 Ma in the isotope correlation plot (^{40}Ar/^{36}Ar = 293 ± 18; mean square weighted deviate (MSWD) = 0.3; Table 3).

[33] Sample 284, from the east Marche fault, is a mylonitic two-mica leucogranite with protomylonitic and ultramylonitic textures. In the protomylonite (sample 284e), four clasts of muscovite give ages varying from 333.8 ± 6.7 Ma to 342.3 ± 4.4 Ma (Figure 4b and Table 2). Micas from pressure shadows and shear bands provide two younger ages than the clasts respectively of 312.2 ± 2.4 Ma and 316.4 ± 5.0 Ma (Figure 4b and Table 2). The ultramylonitic facies yields ages (sample 284c), for newly crystallized micas (see Figure S1b), that range from 339.9 ± 10.1 Ma to 314.3 ± 5.5 Ma (Figure 4c and Table 2). With the exception of the first older age that has a large experimental error and that could result from excess ^{40}Ar contamination by adjacent feldspar, the remaining ages only scatter from 314 to 329 Ma.

[34] Sample 331 is a biotite-sillimanite ± cordierite gneiss that was collected far from the two-mica leucogranites in the Aigurande plateau. Step heating of a single biotite crystal yielded a plateau age of 348.5 ± 4.1 Ma for 95% ^{39}Ar released (Figure 4d and Tables 2 and 3).

5.2. Ouzilly Fault and Surrounding Rocks

[35] Sample 246 is a mylonitic two-mica leucogranite coming from the NW part of the Millevaches massif. Muscovite bulk-separate yielded a plateau age of 313.0 ± 2.8 Ma for 68% of ^{39}Ar released (Figure 4e and Table 4), and an intercept age of 315.3 ± 3.0 Ma in the ^{36}Ar/^{40}Ar versus ^{39}Ar/^{40}Ar isotope plot (Table 3, 40Ar/^{36}Ar of 324 ± 28; MSWD = 0.69).

[36] Sample 241 is a biotite-sillimanite ± cordierite gneiss, collected within the fault, in the NW part of the Millevaches massif. It provides a weighted age of 312.7 ± 3.3 Ma on nine spots from a single biotite grain, with no significant age zoning (Figure 4f and Table 4).

[37] Sample 6 (Figure 4g and Table 4) comes from the NE edge of the Millevaches massif, and is an undeformed two-mica leucogranite. The bulk biotite sample has a discordant age spectrum with apparent ages ranging from 305 to 338 Ma. For 70% of the total ^{39}Ar released, these ages vary between 317 and 322 Ma. The ^{36}Ar/^{40}Ar versus ^{39}Ar/^{40}Ar isotope correlation plot gives an intercept age of 320.8 ± 4.3 Ma with an initial ^{40}Ar/^{36}Ar ratio of 450 ± 47

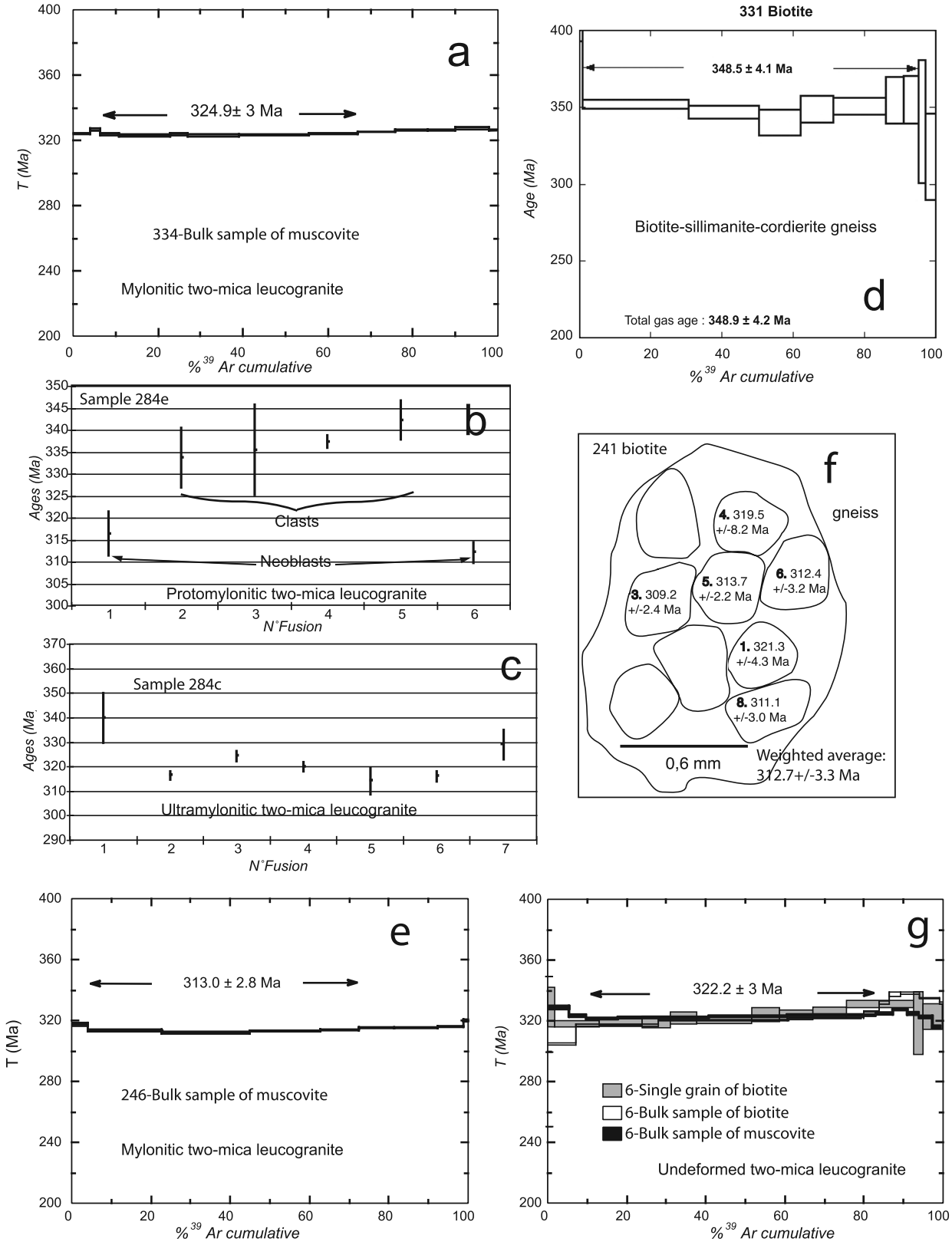

Figure 4. The $^{40}Ar/^{39}Ar$ results for samples 334, 331, 284e, 284c, 246, 241, and 6.

Table 2. The $^{40}Ar/^{39}Ar$ Results for Samples 334, 284e, 284c, and 331[a]

Number of Samples	$^{40}Ar^*/^{39}Ar$	$^{36}Ar/^{40}Ar^*(1000)$	$^{39}Ar/^{40}Ar$	$^{38}Ar/^{39}Ar$	^{39}Ar,%	$^{40}Ar^*$, %	Age, Ma	±1 SD
Sample 334 Bulk Muscovite, J = 0.01401								
1	14.11	0.577	0.0587	0.018	4.2	82.9	325.49	0.69
2	14.24	0.117	0.0677	0.013	6.7	96.4	328.15	0.68
3	14.09	0.08	0.0692	0.013	11.1	97.5	325.04	0.77
4	14.07	0.035	0.0703	0.012	23.4	98.8	324.52	0.72
5	14.09	0.08	0.0692	0.013	27.8	97.5	325.04	0.77
6	14.07	0.035	0.0703	0.012	40	98.8	324.52	0.72
7	14.08	0.018	0.0705	0.012	56.9	99.3	324.79	0.42
8	14.11	0.014	0.0705	0.012	68.4	99.5	325.37	0.4
9	14.17	0.012	0.0702	0.012	77.5	99.5	326.62	0.32
10	14.22	0.008	0.07	0.012	85.4	99.6	327.83	0.32
11	14.22	0.003	0.0702	0.012	92	99.8	327.68	0.45
12	14.27	0.003	0.0699	0.012	100	99.8	328.73	0.51
Sample 284e Polished Section, J = 0.012713								
1	15.08	0.207	0.0622	0		93.9	316.45	5.03
2	15.988	0.069	0.0612	0		98	333.83	6.77
3	16.074	0.134	0.0597	0.026		96.1	335.48	10.28
4	16.178	0.129	0.0594	0.025		96.2	337.45	1.49
5	16.435	0.13	0.0584	0.022		96.2	342.33	4.44
6	14.861	0.131	0.0646	0.001		96.2	312.22	2.37
Sample 284c Polished Section, J = 0.012713								
1	16.311	0.137	0.0588	0.001		96	339.97	10.09
2	15.084	0.188	0.0626	0		94.5	316.51	1.67
3	15.493	0.078	0.063	0		97.7	324.38	2.03
4	15.263	0.137	0.0628	0		96	319.95	1.88
5	14.967	0.137	0.0639	0.001		96	314.26	5.55
6	15.064	0.151	0.0634	0		95.6	316.13	2.12
7	15.74	0.133	0.061	0		96.1	329.09	5.95
Sample 331 Single Biotite Step Heating, J = 0.012713								
1	5.829	20.624	0.0384	0	0	22.4	128.98	394.54
2	13.735	0.846	0.0545	0	0.1	75	290.36	71.8
3	16.263	0.059	0.0604	0	2.2	98.3	339.07	6.1
4	17.925	0.063	0.0547	0	4	98.1	370.37	26.75
5	15.516	0.248	0.0597	0.003	13.9	92.7	324.81	2.58
6	16.402	0.066	0.0597	0.03	20.1	98.1	341.71	3.55
7	16.854	0.073	0.058	0	23.8	97.8	350.27	5.55
8	16.273	0.012	0.0612	0.109	28.7	99.6	339.26	7.08
9	16.07	0.058	0.0611	0.022	44.5	98.3	335.4	1.89
10	16.084	0.09	0.0605	0.008	53.9	97.3	335.65	2.49
11	16.654	0.005	0.0599	0	83	99.8	346.48	1.94
12	16.436	0.066	0.0596	0.037	88.9	98	342.35	5.51
13	16.977	0.025	0.0584	0.021	96.5	99.2	352.58	5.43
14	16.295	0.123	0.0591	0.077	100	96.3	339.67	10.85

[a]Ar* indicates radiogenic Ar.

Table 3. The $^{40}Ar/^{39}Ar$ Synthetic Results for Bulk Sample, Single Grain, and Polished Section

Sample	Total Age, Ma	Plateau Age, Ma	Isochron Age, Ma	$^{40}Ar/^{36}Ar$	MSWD
334, bulk muscovite sample	324.6 ± 3	324.9 ± 3	326.9 ± 3.0	293 ± 18	0.3
331, single biotite step heating	348.9 ± 4.2	348.5 ± 4.1			
246, bulk muscovite sample	308.0 ± 2.8	313.0 ± 2.8	315.3 ± 3.0	324 ± 28	0.69
6, bulk biotite sample	320.0 ± 2.9		320.8 ± 4.3	450 ± 47	1.71
6, bulk muscovite sample	317.9 ± 2.9	322.2 ± 3			
6, single biotite step heating	329.7 ± 3.4		322.8 ± 3.5	299 ± 37	2.17
40, single biotite step heating	313.2 ± 3.3		316.3 ± 3.5	347 ± 93	2.1
347, bulk biotite sample	334.3 ± 3.1	341.4 ± 3.2			
356, bulk muscovite sample	310.5 ± 2.8	310.2 ± 2.9	313.7 ± 3.1	249 ± 11	1.92
404, bulk biotite sample	312.0 ± 2.9		318.6 ± 3.8	314 ± 45	5.64

Table 4. The $^{40}Ar/^{39}Ar$ Results for Samples 246, 241, 6

Number of Samples	$^{40}Ar^*/^{39}Ar$	$^{36}Ar/^{40}Ar^*(1000)$	$^{39}Ar/^{40}Ar$	$^{38}Ar/^{39}Ar$	^{39}Ar,%	$^{40}Ar^*$, %	Age, Ma	±1 SD
			Sample 246 Bulk Muscovite, J = 0.01401					
1	13.75	0.429	0.0634	0.018	5.5	87.2	317.77	1.08
2	13.54	0.042	0.0728	0.012	24.1	98.6	313.47	0.55
3	13.48	0.011	0.0738	0.012	46.4	99.5	312.07	0.52
4	13.53	0.013	0.0735	0.012	63.8	99.5	313.19	0.22
5	13.57	0.011	0.0733	0.012	73.6	99.5	313.95	0.38
6	13.62	0.004	0.0732	0.012	82.6	99.7	315.1	0.44
7	13.63	0	0.0732	0.012	93.5	99.9	315.33	0.35
8	13.67	0	0.073	0.011	100	99.9	316.19	0.42
			Sample 241 Single Biotite Spot Fusion, J = 0.012713					
1	15.084	0.067	0.065	0.006		99.7	316.5	4.23
2	15.018	0.04	0.0657	0.007		98.9	315.24	3.34
3	14.703	0.067	0.0666	0.011		98.1	309.16	2.36
4	15.239	0.126	0.0631	0.007		96.3	319.5	8.22
5	14.94	0.043	0.066	0.007		98.8	313.73	2.17
6	14.868	0.067	0.0659	0.005		98.1	312.36	3.2
7	14.628	0.072	0.0669	0.007		97.9	307.71	4.1
8	14.805	0.043	0.0666	0.006		98.8	311.14	3.04
9	14.978	0.066	0.0653	0.007		98.1	314.47	5.76
			Sample 6 Bulk Biotite, J = 0.01401					
1	13.13	0.675	0.0609	0.035	7.4	20.1	304.68	0.94
2	13.72	0.11	0.0704	0.033	28.3	3.4	317.12	0.47
3	13.87	0.033	0.0713	0.032	61.1	1.1	320.28	0.42
4	13.95	0.029	0.071	0.032	80.1	1	321.98	0.46
5	14.15	0.143	0.0676	0.034	83.8	4.4	326.26	0.66
6	14.43	0.323	0.0626	0.034	86.6	9.7	332.2	1.02
7	14.69	0.397	0.06	0.035	89.3	11.9	337.59	1.22
8	14.72	0.295	0.0619	0.034	94	8.8	338.23	0.75
9	14.56	0.146	0.0656	0.03	99	4.4	334.86	0.64
10	14.4	0.059	0.0681	0.032	100	1.8	331.59	0.81
			Sample 6 Bulk Muscovite, J = 0.01401					
1	14.26	0.605	0.0575	0.019	5.4	82	328.55	0.96
2	14	0.06	0.0701	0.014	9.8	98.1	323.13	0.8
3	13.91	0.03	0.0711	0.013	17.9	99	321.26	0.39
4	13.93	0.014	0.0714	0.013	41.7	99.5	321.63	0.44
5	13.96	0.008	0.0713	0.013	62.1	99.6	322.35	0.4
6	14	0.009	0.0711	0.013	77.3	99.6	323.16	0.49
7	14	0.012	0.0711	0.013	85.2	99.5	323.02	0.43
8	14.05	0.009	0.0709	0.013	89.4	99.6	324.26	0.63
9	14.19	0.004	0.0703	0.011	93.4	99.8	327.13	0.5
10	14.05	0	0.0711	0.012	96.3	99.9	324.23	0.62
11	13.95	0.018	0.0712	0.014	100	99.3	321.96	0.66
			Sample 6 Single Biotite Step Heating, J = 0.012713					
1	49.119	1.575	0.0108	0.046	1	53.5	875.32	22.42
2	15.736	0.93	0.046	0.018	2.4	72.6	329.02	13.14
3	15.174	0.262	0.0607	0.017	13.5	92.3	318.24	2.28
4	15.216	0.065	0.0644	0.02	24.5	98.1	319.05	2.28
5	15.223	0.01	0.0653	0.019	31.5	99.7	319.19	4.22
6	15.378	0,011	0.0648	0.021	38.1	99.7	322.16	4.14
7	15.302	0.014	0.065	0.02	51.8	99.6	320.71	2.19
8	15.475	0.002	0.0644	0.021	58.9	100	324.02	4.57
9	15.479	0.001	0.0644	0.019	67.3	100	324.11	3.26
10	15.578	0.01	0.0639	0.021	75.8	99.7	325.99	3.54
11	15.849	0.035	0.0624	0.009	92.7	99	331.17	2.35
12	15.191	0.073	0.0643	0.015	94.6	97.9	318.58	21.07
13	15.406	0.01	0.0646	0.017	99.9	99.7	322.7	8.2
7	13.48	0.061	0.0727	0.055	63.8	98.1	312.08	0.59
8	13.5	0.036	0.0732	0.056	69.1	98.8	312.41	0.51
9	13.5	0.018	0.0736	0.056	80.1	99.3	312.41	0.44
10	13.55	0.013	0.0734	0.056	96.3	99.5	313.52	0.45
11	13.53	0.022	0.0734	0.057	100	99.2	313.09	0.38

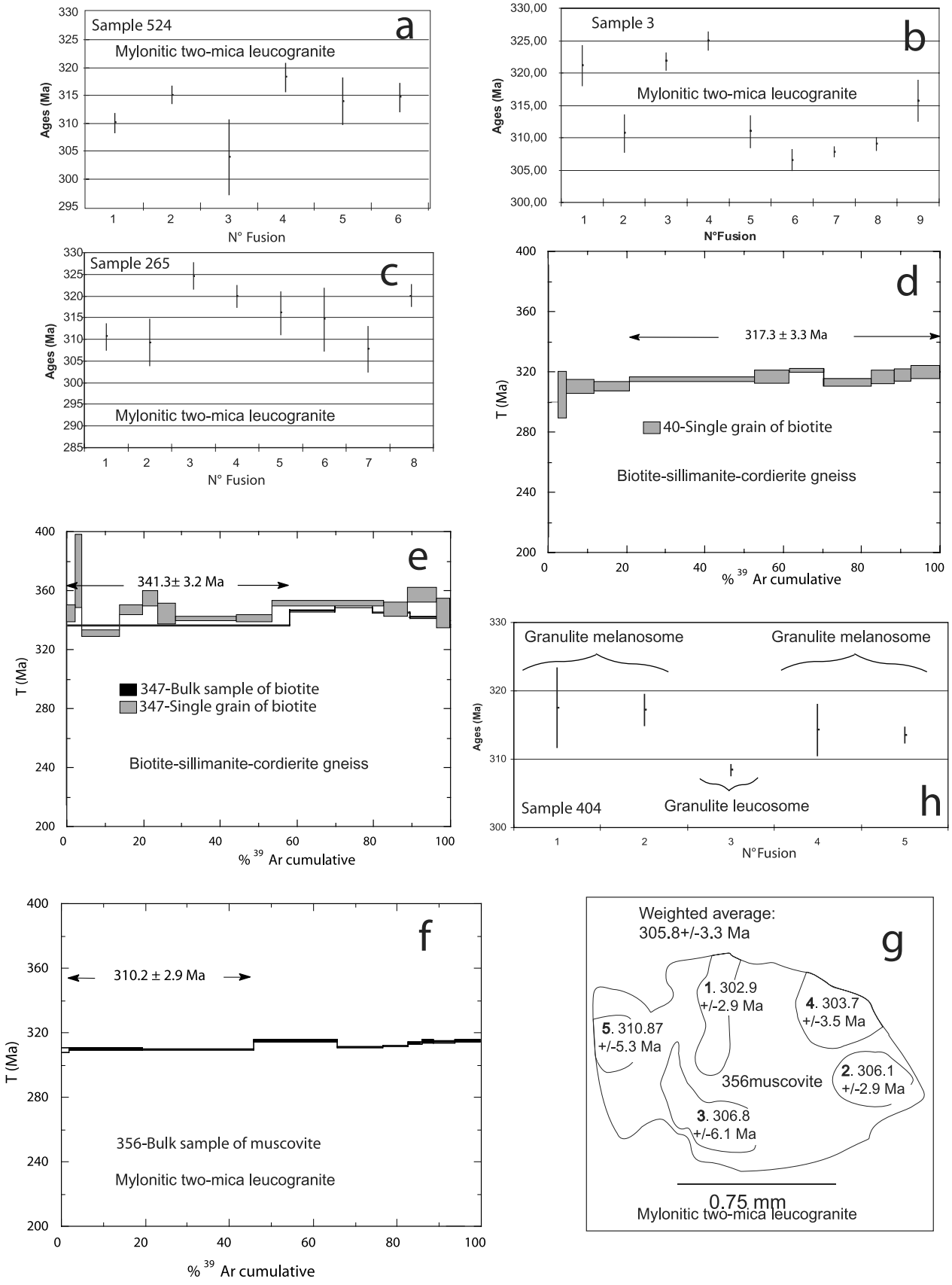

Figure 5. The $^{40}Ar/^{39}Ar$ results for samples 524, 3, 265, 40, 347, 356, and 404.

Table 5. The $^{40}Ar/^{39}Ar$ Results for Samples 524, 3, 265, 40, and 347

Number of Samples	$^{40}Ar^*/^{39}Ar$	$^{36}Ar/^{40}Ar^*(1000)$	$^{39}Ar/^{40}Ar$	$^{38}Ar/^{39}Ar$	^{39}Ar,%	$^{40}Ar^*$, %	Age, Ma	±1 SD
			Sample 524 Polished Section, J = 0.014019					
1	13.379	0.097	0.073	0		97.1	310.11	1.72
2	13.612	0.094	0.071	0		97.2	315.07	1.56
3	13.086	0.221	0.071	0		93.5	303.86	6.79
4	13.762	0.117	0.07	0		96.5	318.26	2.6
5	13.558	0.168	0.07	0		95.1	313.93	4.17
6	13.592	0.188	0.069	0		94.5	314.65	2.48
			Sample 3 Polished Section, J = 0.012713					
1	15.323	0.06	0.0639	0		98.2	321.11	3.06
2	14.781	0.329	0.061	0.001		90.3	310.68	2.87
3	15.358	0.031	0.0644	0		99.1	321.78	1.29
4	15.523	0.059	0.0632	0		98.2	324.95	1.39
5	14.794	0.142	0.0647	0.003		95.8	310.93	2.47
6	14.567	0.121	0.0661	0		96.4	306.54	1.61
7	14.632	0.152	0.0652	0		95.5	307.8	0.76
8	14.695	0.556	0.0568	0.007		83.6	309.01	1
9	15.041	0.035	0.0657	0		99	315.68	3.16
			Sample 265 Polished Section, J = 0.012713					
1	14.775	0.187	0.0639	0.005		94.5	310.55	3.14
2	14.707	0.794	0.052	0.005		96.2	309.24	5.35
3	15.506	0.07	0.0631	0		97.9	324.61	3.09
4	15.263	0.153	0.0625	0.001		95.5	319.96	2.5
5	15.06	0.13	0.0638	0.014		96.2	316.05	4.91
6	14.984	0.129	0.0641	0		96.2	314.59	7.2
7	14.627	0.225	0.0638	0.001		93.3	307.7	5.17
8	15.269	0.267	0.0603	0.003		92.1	320.08	2.52
			Sample 40 Single Biotite Step Heating, J = 0.012713					
1	114.734	0.064	0.0085	0.062	0	98.1	1622.99	136.21
2	0.991	3.246	0.0411	0.096	0.6	4.1	22.6	53.39
3	5.738	1.926	0.075	0.002	2.2	43.1	127.04	19.9
4	14.485	0.126	0.0664	0.016	4	96.3	304.95	16.9
5	14.77	0.109	0.0655	0.028	11.3	96.8	310.45	5.21
6	14.797	0.038	0.0668	0.033	20.5	98.9	310.99	3.59
7	15.058	0.043	0.0655	0.019	52.4	98.8	316.01	1.61
8	15.149	0.115	0.0637	0.026	61.2	96.6	317.77	5.22
9	15.393	0.036	0.0642	0.024	70.1	99	322.45	1.81
10	14.923	0.166	0.0637	0.018	82.5	95.1	313.42	2.81
11	15.145	0.214	0.0618	0.025	88.2	93.7	317.68	4.98
12	15.228	0.087	0.0639	0.084	92.5	97.5	319.28	4.28
13	15.33	0.166	0.062	0.015	99.9	95.1	321.23	4.91
			Sample 347 Single Biotite Step Heating, J = 0.012713					
1	22.292	0.117	0.0433	0.028	1.2	96.5	450.15	57.67
2	16.922	0.006	0.0589	0	30.7	99.8	351.54	2.98
3	16.644	0.022	0.0596	0	50.5	99.3	346.29	4.24
4	16.29	0.102	0.0595	0	62.3	97	339.58	8.25
5	16.756	0.008	0.0595	0	71.5	99.7	348.41	8.57
6	16.841	0.002	0.0593	0.001	86	99.9	350.01	5.44
7	17.056	0.007	0.0584	0	91.1	99.8	354.07	14.84
8	17.073	0.028	0.058	0.008	95.3	99.2	354.39	15.59
9	16.318	0.021	0.0608	0	97.2	99.4	340.12	40.02
10	15.14	0.28	0.0605	0	99.9	91.7	317.59	28.08
			Sample 347 Bulk Biotite, J = 0.01401					
1	14.63	0.084	0.0666	0.015	58.1	97.4	336.29	0.59
2	15.1	0.017	0.0658	0.014	69.8	99.4	346.22	0.42
3	15.24	0.039	0.0648	0.015	79.6	98.7	349.07	0.44
4	15.06	0.029	0.0658	0.015	89.5	99	345.36	0.48
5	14.88	0.026	0.0666	0.015	97	99.1	341.62	0.63
6	14.61	0.039	0.0675	0.017	100	98.7	336.05	0.73

Table 6. The $^{40}Ar/^{39}Ar$ Results for Samples 356 and 404

Number of Samples	$^{40}Ar^*/^{39}Ar$	$^{36}Ar/^{40}Ar^*(1000)$	$^{39}Ar/^{40}Ar$	$^{38}Ar/^{39}Ar$	^{39}Ar,%	$^{40}Ar^*$, %	Age, Ma	±1 SD
Sample 356 Bulk Muscovite, J = 0.01401								
1	13.38	0.616	0.061	0.023	2.2	81.7	309.96	1.36
2	13.41	0.023	0.074	0.013	19.6	99.2	310.59	0.5
3	13.39	0.006	0.0744	0.012	46.2	99.7	310.14	0.27
4	14.45	0.008	0.0689	0.013	65.8	99.6	332.66	17.6
5	13.47	0.012	0.0738	0.012	76.7	99.5	311.94	0.43
6	13.49	0.008	0.0738	0.013	82.9	99.6	312.32	0.61
7	13.58	0	0.0735	0.012	86.1	99.9	314.31	0.71
8	13.63	0	0.0732	0.011	88.9	99.9	315.38	0.91
9	13.62	0	0.0733	0.011	93.8	99.9	315.11	0.54
10	13.65	0	0.0732	0.011	100	99.9	315.67	0.52
Sample 356 Single Muscovite Spot Fusion, J = 0.012713								
1	14.383	0.152	0.0663	0		95.5	302.97	2.91
2	14.546	0.084	0.067	0		97.5	306.14	2.97
3	14.581	0.09	0.0666	0		97.4	306.81	6.11
4	14.422	0.049	0.0683	0		98.6	303.72	3.56
5	14.792	0.065	0.066	0.026		98.1	310.87	5.3
Sample 404 Polished Section Granulite Paleosome, J = 0.01401								
1	13.727	0.041	0.072	0.025		98.8	317.52	5.84
2	13.711	0.032	0.072	0.023		99.1	317.17	2.28
4	13.575	0.047	0.073	0.021		98.6	314.29	3.74
5	13.536	0.02	0.073	0.022		99.4	313.5	1.14
Sample 404 Polished Section Granulite Leucosome								
3	13.298	0.043	0.074	0.036		98.7	308.38	0.81

(Table 3), which suggests the presence of some excess ^{40}Ar, possibly linked with the partial chloritization of the biotite and trapping of interstitial fluids. A single crystal of biotite gives an age spectrum less disturbed than the bulk sample one, with ages increasing from 318 to 331 Ma. The $^{36}Ar/^{40}Ar$ versus $^{39}Ar/^{40}Ar$ isotope correlation plot gives an intercept age of 322.8 ± 3.5 Ma with an initial $^{40}Ar/^{36}Ar$ ratio of 299 ± 37 (Table 3). The bulk muscovite sample yields a plateau age of 322.2 ± 3.0 Ma for 70% of the total ^{39}Ar released (Table 3).

[38] Samples 524 and 3 are mylonitic two-mica leucogranites, collected on the NE edge of the Millevaches massif. Shear criteria indicate sinistral sense of shearing. Thin polished rock sections have been used for in situ laser probe $^{40}Ar/^{39}Ar$ dating. Small secondary micas within shear bands give ages ranging from 303.8 ± 6.7 Ma to 318.3 ± 2.6 Ma on sample 524 (Figure 5a and Table 5), and from 306.5 ± 1.6 Ma to 325.0 ± 1.4 Ma on sample 3 (Figure 5b and Table 5).

[39] Sample 265 is a mylonitic two-mica leucogranite that records a southwest directed reverse faulting event on the NE edge of the Millevaches massif. Muscovites from a polished rock section give in situ ages ranging from 307.7 ± 5.2 Ma to 324.6 ± 3.1 Ma (Figure 5c and Table 5). Ages obtained from recrystallized shear zones within this section only vary from 310.5 ± 3.1 Ma to 316.0 ± 4.9 Ma.

[40] Sample 40 is a biotite-sillimanite ± cordierite gneiss collected from within the Felletin fault on the eastern edge of the Millevaches massif. A single crystal of biotite yields a plateau age of 317.3 ± 3.3 Ma for 80% of ^{39}Ar released (Figure 5d and Table 5). The isochron gives an age of 316.3 ± 3.5 Ma with an initial $^{40}Ar/^{36}Ar$ ratio of 347 ± 93 (MSWD = 2.1, Table 3).

[41] Sample 347 is a biotite-sillimanite ± cordierite gneiss collected from the southeastern part of the La Courtine fault, far from the two-mica leucogranites. The bulk biotite sample yields a discordant age spectrum with a first step at 341.3 ± 3.2 Ma for 58% of ^{39}Ar released (Figure 5e and Tables 3 and 5). The remaining part of the spectrum has a convex pattern with a maximum age of 349.0 ± 0.4 and a minimum one of 336 Ma at 1400°C. The age spectrum of a single biotite grain irregularly increases from 324 to 352 Ma.

5.3. Pradines Fault

[42] The bulk muscovite sample from a C-S mylonite (sample 356) yields an age of 310.2 ± 2.9 Ma for 46% of released ^{39}Ar (Figure 5f and Tables 3 and 6). After a bump close to 320 Ma, the following steps give ages between 312 and 315.5 Ma. An intercept age of 313.7 ± 3.1 Ma has been calculated with a MSWD of 1.92 (Table 3). Five spot fusion ages obtained on a single muscovite grain from the same sample range between 303.0 ± 3.0 Ma and 310.9 ± 5.3 Ma (Figure 5g and Table 6).

[43] Sample 404 is a micaschist which has experienced granulitic metamorphism. It was collected within the Pradines fault in the northern part of the Millevaches massif. Biotites from polished melanosomes give ages varying between 313.5 ± 1.0 Ma and 317.5 ± 5.8 Ma (Figure 5h and fusions 1, 2, 4, and 5 and Table 6). Biotites from the

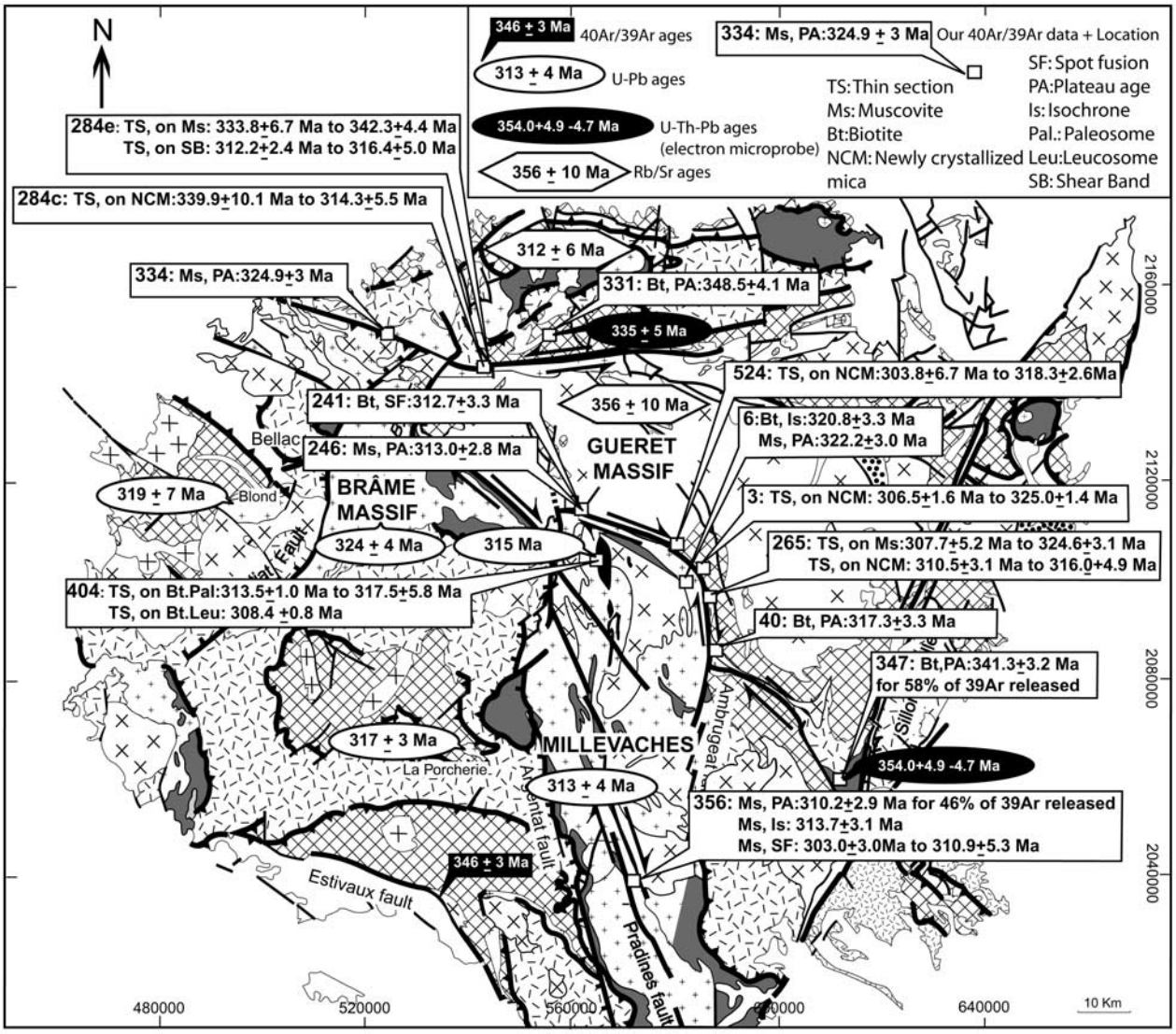

Figure 6. Geological map of the Limousin area showing the location and the new $^{40}Ar/^{39}Ar$ dates (boxes). U-Pb previous age data (zircon and monazite) are mentioned by oval shapes, Brâme massif [*Holliger et al.*, 1986], Porcherie two-mica leucogranite [*Lafon and Respaut*, 1988], Millevaches massif [*Gébelin*, 2004], and Blond two-mica leucogranite [*Alexandrov et al.*, 2000]. Rb/Sr previous age data (on whole rock) are distinguished by hexagon, Guéret biotite-bearing granite [*Berthier et al.*, 1979], Aigurande plateau two-mica leucogranite [*Petitpierre and Duthou*, 1980]. Previous $^{40}Ar/^{39}Ar$ data and U-Th-Pb using electron microprobe [*Gébelin*, 2004] are noted by black box [*Roig et al.*, 1996] and by black oval shapes, respectively.

leucosome give an age of 308.4 ± 0.8 Ma (Figure 5h and fusion 3 and Table 6).

6. Discussion of Argon Data and Comparison With Other Geochronological Data

[44] The $^{40}Ar/^{39}Ar$ mica ages are generally interpreted to record cooling at temperature ranging from about 400°C for muscovite [*Hames and Bowring*, 1994; *Dahl*, 1996] to 300°C for biotite [*Harrison et al.*, 1985]. Therefore our $^{40}Ar/^{39}Ar$ ages cannot be used directly to date the emplacement of the various granites or the peak metamorphic conditions in the country rocks of these granites. However, in an attempt to better constrain the cooling path of the Limousin granitic and metamorphic rocks, several U-Pb and U-Th-Pb ages have been obtained using Thermal Ionization Mass Spectrometer (TIMS) and electron microprobe techniques on various lithologies [*Gébelin*, 2004]. In the following, we discuss these ages because they provide key information for the interpretation of the new $^{40}Ar/^{39}Ar$ dates in terms of cooling versus crystallization ages (Figure 6). For most investigated granites and metamorphic rocks, the

U-Pb and $^{40}Ar/^{39}Ar$ ages are characterized by overlapping and small error margins, which suggests that relatively fast rates of cooling prevailed in the area during the Carboniferous.

[45] To the north of the Marche fault, a biotite from Bt-Sil ± Cd gneisses of Aigurande plateau (sample 331) yielded a plateau age of 348 ± 4 Ma. This age is interpreted as a cooling age postdating high-temperature deformation marked by biotite and sillimanite shear bands (see Text S1, section 3). The $^{40}Ar/^{39}Ar$ ages of *Boutin and Montigny* [1993] [389 ± 8 Ma] are interpreted as cooling ages of amphibole at a closure temperature ~550°C [*Dahl*, 1996]. When considered together with our new biotite age, this points to an average cooling rate of 6 +2.6/−1.5°C/Myr between 390 and 350 Ma. It must be noted that, in this area, the biotite K-Ar chronometer has neither been influenced by the emplacement of the 312 Ma leucogranites [*Petitpierre and Duthou*, 1980] or by shearing along the Marche fault. This $^{40}Ar/^{39}Ar$ age of circa 350 Ma is consistent with the ones found in the south Limousin on synkinematic granite biotites [*Roig et al.*, 1996] and in the Monts du Lyonnais on the Grand Chemin strike-slip fault [*Costa et al.*, 1993].

[46] For the synkinematic, mylonitic two-mica leucogranites of the Marche fault (samples 284c and 284e, sample 334), two different $^{40}Ar/^{39}Ar$ age groups have been recognized. The older group at circa 340 Ma (sample 284e), derived from muscovite porphyroclasts from a protomylonitic leucogranite, is interpreted to represent the cooling age of the two-mica leucogranites at approximately 400°C in the EMF. A similar U-Th-Pb age of 335 ± 5 Ma has been obtained on monazite by electron microprobe from this sample [*Gébelin*, 2004]. This age is interpreted to represent the emplacement age of the two-mica leucogranites during the sinistral strike-slip shearing activity in EMF. A second generation of tiny synkinematic muscovite, in the pressure shadows of primary muscovite porphyroclasts and in ultramylonitic facies, yields $^{40}Ar/^{39}Ar$ ages in the range 315–320 Ma (results obtained in situ on polished thin rock sections using laser probe; see Appendix A). Given these microstructural relationships and the relatively low-temperature conditions (~300°C) that dominate at the end of deformation (see Text S1, section 1), these 315–320 Ma ages are interpreted as crystallization ages marking the end of sinistral shear along the eastern Marche fault. To the west, a northeast directed sinistral-reverse movement is recorded by the Marche fault. There, a mylonitic leucogranite (sample 334) yielded a muscovite plateau date of circa 325 Ma. It must be noted that this age was obtained on a bulk mineral separate that likely corresponds to a mixture of primary and newly formed muscovites of unknown proportion. Therefore we consider that the age of circa 325 Ma represents a maximum age for the last stage of deformation along the WMF. As a whole, the Marche fault recorded movement from about 340 to 315 Ma.

[47] Most $^{40}Ar/^{39}Ar$ sampling focused on the southeastern portion of the Ouzilly fault because of the quality of exposures and its geometry and kinematics that have been influenced by the emplacement of the Millevaches granites. Both deformed and undeformed samples were collected along this fault. Biotite and muscovite from the Millevaches undeformed two-mica leucogranite (sample 6) have overlapping plateau ages of 320–322 Ma, which indicates fast cooling between 300 and 400°C. This age is consistent with the U-Pb zircon age of the Brâme leucogranite dated at 324 ± 4 Ma [*Holliger et al.*, 1986].

[48] For the mylonitic two-mica leucogranites (samples 3, 246, 265, and 524), muscovite displays a distribution of ages from 305 to 325 Ma, similar to that reported by *Scaillet et al.* [1996a] for the Brâme massif. It is worth noting that the dextrally sheared two-mica leucogranites (sample 246) and the sinistrally sheared ones (samples 524 and 3) display similar ages. Biotites from sillimanite-cordierite gneisses deformed along the fault (samples 40 and 241) yield consistent plateau dates of circa 315 Ma. Away from the fault, biotite from a similar gneiss (sample 347) has a discordant age spectrum that increases from 324 to 352 Ma. Monazite from this biotite-sillimanite-cordierite gneiss provides a U-Th-Pb age of 354.0 ± 4.9/−4.7 Ma [*Gébelin*, 2004] which is interpreted as a crystallization age during the high-temperature metamorphism. Therefore the discordant age pattern of sample 347 likely results from the partial resetting of a 350 Ma metamorphic biotite during the emplacement of the Millevaches two-mica leucogranites and subsequent dextral shearing. It has been demonstrated on microstructural grounds that this shearing occurred during the cooling of the leucogranite (section 4) under a temperature range of 700–400°C. Micas from mylonitic granites and gneisses give $^{40}Ar/^{39}Ar$ ages that are circa 10 Myr younger than the mica ages from undeformed granites. The scattering of muscovite ages within the shear zones (305–325 Ma) probably results from several effects: (1) partial resetting of magmatic muscovites; (2) diachronous exhumation/cooling along the Ouzilly fault; (3) activation of the dextral strike-slip fault; (4) fluid migration along the contact; (5) contamination by adjacent minerals during in situ laser probe experiments; and (6) analytical artefacts (e.g., argon recoil). Nonetheless, we suggest that the end of dextral shear along the Ouzilly fault can be placed at 310–315 Ma, when the sheared rocks cooled below 300–400°C. This interpretation is confirmed by the data obtained along the Pradines fault. There, a syntectonic two-mica leucogranite with C-S fabrics gives a U-Pb zircon and monazite age of 313 ± 4 Ma [*Gébelin*, 2004]. Step heating and in situ laser probe $^{40}Ar/^{39}Ar$ dating of muscovite yield ages that range from 305 to 315 Ma (sample 356) which points to very fast rates of cooling after granite emplacement and coeval deformation, given the closure temperature difference between K-Ar in muscovite (400°C [*Hames and Bowring*, 1994; *Dahl*, 1996]) and U-Pb in monazite (600–750°C [*Copeland et al.*, 1988; *Parrish*, 1990]). Because of this fast cooling, the $^{40}Ar/^{39}Ar$ ages nearly coincide with that of deformation and this is likely to be the case for the Ouzilly fault. Indeed, these fast cooling rates also prevailed further north along the Pradines fault where small bodies of granulitic rocks were exhumed. TIMS U-Pb dating of zircon and monazite provides ages of 315 ± 4 Ma and 316 ± 2 Ma, respectively, for the melanosome and leucosome parts of these granulites

[*Gébelin*, 2004]. Biotite from the same sample has in situ laser probe ages between 308 and 317 Ma (sample 404). These ages are interpreted as a minimum age for the granulitic metamorphism and subsequent anatexis recorded by these small bodies that experienced fast exhumation and cooling, contemporaneously with the synkinematic emplacement of the Pradines leucogranite.

[49] To summarize, the new $^{40}Ar/^{39}Ar$ ages, along with U-Pb and U-Th-Pb ages [*Gébelin*, 2004], suggest that the Millevaches two-mica leucogranites were emplaced at circa 325–320 Ma in a dextral strike-slip setting while the Guéret biotite granite had already cooled by 335 Ma [*Faure et al.*, 2002]. Strike-slip shear continued until 315–310 Ma as recorded by mylonitic rocks collected along the E-NE edge of the Millevaches massif (Ouzilly fault) and within the massif itself (Pradines fault). These mylonitic rocks display a dominant dextral kinematics, with the exception of some sinistral strike-slip faults that are considered as conjugated faults of the main Ouzilly fault. In addition, southwest directed reverse shearing was also recorded along the NE edge of the Millevaches massif (sample 265) but the $^{40}Ar/^{39}Ar$ ages are similar to those recorded by dextral and conjugated sinistral shear zones. This implies a localized NE-SW compression in the NE edge of the Millevaches massif at the end of the Millevaches leucogranite emplacement (Figures 1 and 2). Locally, strike-slip movements could be responsible for the exhumation of lower crustal rocks. Comparing $^{40}Ar/^{39}Ar$ ages with U-Pb and U-Th-Pb ages suggests that fast cooling rates prevailed during this exhumation. It is worth noting that similar ages of 314 ± 5 Ma (U-Pb method [*Mougeot et al.*, 1997]) have been obtained from the leucosomes of metatexites structurally connected to larger laccoliths of leucogranites emplaced within detachment zones on the Velay anatectic dome in the French Massif Central. Compared with the Marche fault that acted between 340 and 315 Ma, the shearing along the Ouzilly (and Pradines) fault appears to be restricted to a shorter time interval between 325 and 310 Ma. However, there is much evidence to show that the movement along the Ouzilly shear zone already took place during, or shortly before, the emplacement of the biotite-bearing granites: (1) quartz preferred orientations in biotite-bearing granite (Guéret type) recording a ductile deformation between 400° and 700°C, (2) the dextrally sheared biotites of biotite-sillimanite ± cordierite gneisses (sample 347) revealing cooling age of 350 Ma, and (3) the $^{40}Ar/^{39}Ar$ ages of 346 ± 3 Ma (on biotite [*Roig et al.*, 1996]) attesting to strike-slip fault activity. This suggests continuous strike-slip shear from around 350–310 Ma.

7. Relationships Between the South Armorican Shear Zone and the Limousin Shear Zones

[50] The Armorican Massif and the Limousin region present similarities in their nature, structure, and age of geological units. The NW-SE trend observed from the Brittany Cap to southern Brittany may extend as far as the Limousin region. Drilling through the ''Seuil du Poitou'' (ANDRA project [*Virlogeux et al.*, 1999]) shows that the SASZ extends under the Mesozoic sedimentary cover and merges with the Limousin faults. The Cholet faults are in continuity with the Marche fault system, whereas the Ouzilly fault system is the southeastern continuation of the Bressuire and Partenay faults (Figure 7b).

[51] Recent argon thermochronology works [*Le Carlier de Veslud et al.*, 2004] attest of a major calc-alkaline event in the ''Seuil du Poitou'' around 350 Ma, synchronous with the emplacement of the Guéret-type granites in the northern Limousin. The ''Seuil du Poitou'' granites are also spatially associated with faults [*Le Carlier de Veslud et al.*, 2004] that connect the South Armorican Massif to the Limousin region (Figures 7a and 7b).

[52] In the northern branch of the North Armorican Shear Zone, leucogranites recorded the end of wrench tectonics at 312 ± 3 Ma [*Gumiaux et al.*, 2004a]. The Allaire massif (Figure 7b), in the SASZ, yields $^{40}Ar/^{39}Ar$ cooling ages between 312 and 305 Ma (G. Ruffet, unpublished data as cited by *Gumiaux et al.* [2004a]). This agrees with our new $^{40}Ar/^{39}Ar$ data for the Limousin region that record the end of fault movement around 300 Ma.

[53] Syntectonic granites of the SASZ are dated at 313 ± 15 Ma [*Bernard-Griffiths et al.*, 1985; *Jégouzo and Rosello*, 1988]. Just north of the SASZ (Figure 7), intrusion yields a U-Pb zircon age of 315–325 Ma. South of the south Brittany domain, two-mica leucogranites were emplaced around 305–300 Ma [*Bernard-Griffiths et al.*, 1985]. All of these ages agree with our $^{40}Ar/^{39}Ar$ cooling ages of 320 and 313 Ma from the two-mica leucogranites on the NE edge of the Millevaches massif and from the Brâme massif, respectively. These ages are the same as the emplacement ages of numerous Limousin two-mica leucogranites at 310–330 Ma [*Holliger et al.*, 1986; *Lafon and Respaut*, 1988; *Alexandrov et al.*, 2000; *Gébelin*, 2004].

[54] These data suggest that the Limousin region and the South Armorican Massif underwent two major granitic events contemporaneous with strike-slip tectonics: first, a voluminous calc-alkaline magmatic event at circa 350 Ma, and second, a crustal melting event at circa 320 Ma. Late increment of deformation recorded by the $^{40}Ar/^{39}Ar$ system in biotites is estimated at about 300 Ma for the South Armorican Massif [*Gumiaux et al.*, 2004a] and for the Limousin (our new data). These results are consistent with the fact that Stephanian sedimentary formations have been sheared by the SASZ [*Rolin and Colchen*, 2001], thus placing the final movements around 290 Ma. Therefore E-W to NW-SE striking Limousin mylonitic zones represent the southeastern extension of the SASZ (Figure 7b).

8. Transpressive Setting and Magma Emplacement Hypothesis

8.1. Transpressive Setting Evidences

[55] Many features observed within the Limousin granite plutons call for an emplacement in a transpressive setting. The Limousin plutons are spatially associated with major synmagmatic dextral strike-slip shear zones. A continuous 1- to 5-km-wide band of orthogneisses and mylonites

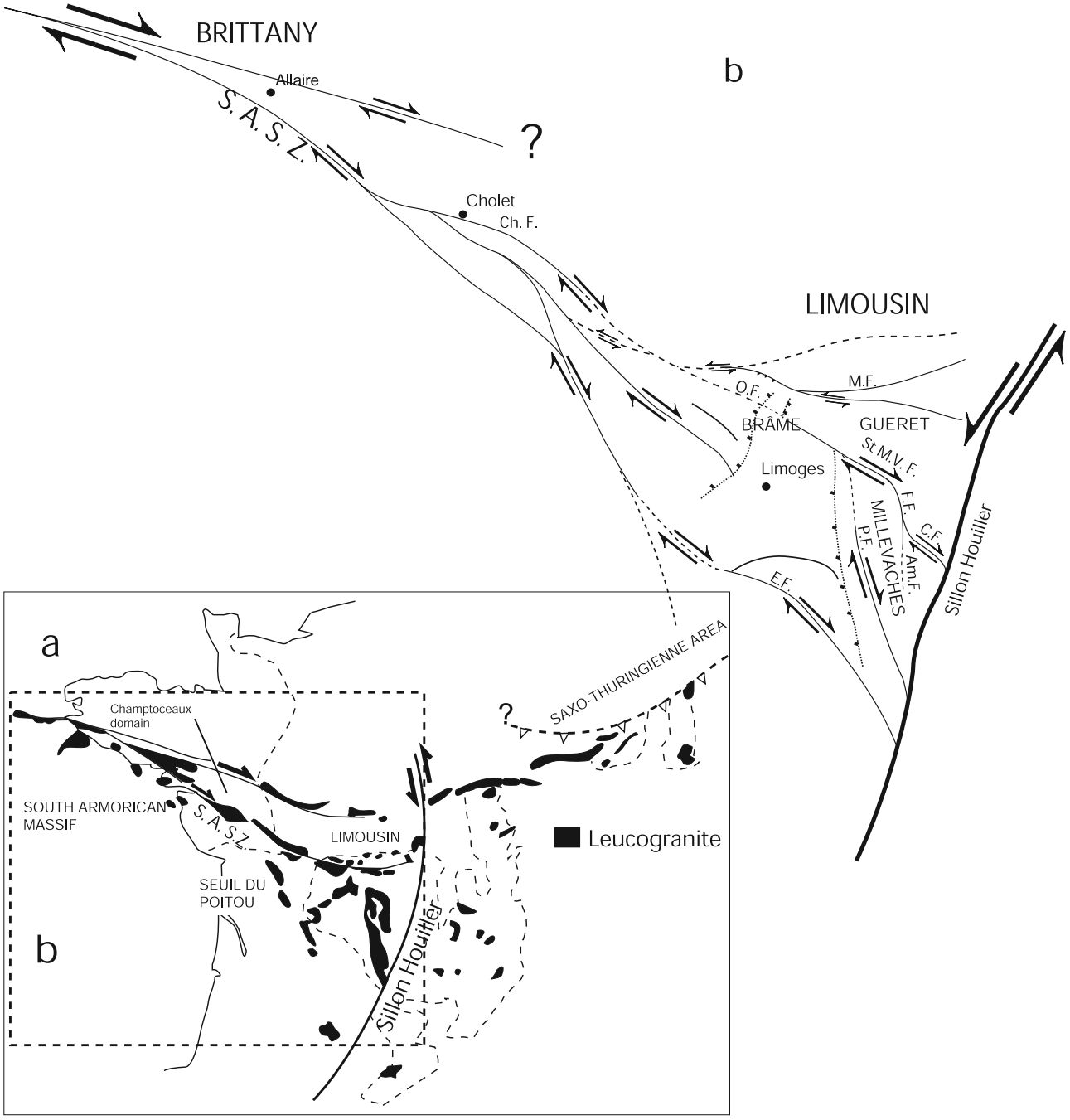

Figure 7. (a) Map of leucogranites in France according to *Autran and Lameyre* [1980]. (b) Map of relationships between South Armorican shear zones and Limousin shear zones showing half of a possible pop-up structure, S.A.S.Z., South Armorican Shear Zone; Ch. F., Cholet fault; O.F., Ouzilly fault; P.F., Pradines fault; St M.V.F., St Michel de Veisse fault; Am.F, Ambrugeat fault; F.F., Felletin fault; C.F., Courtine fault; E. F., Estivaux fault; M.F., Marche fault.

characterizes most of the shear zones. Granites display horizontal lineation and vertical foliation associated with dextral strike-slip kinematic criteria (C-S, asymmetric tails, shear bands, etc.) that indicate a component of noncoaxial deformation with an horizontal shear direction. Local down-dip lineation and sinistral strike-slip kinematic criteria underlined by similar microstructures as the dominant dextral strike-slip component have been detected in the EMF (Figure 1). These observations are consistent with a component of coaxial deformation with a vertical stretching direction. The combination of coaxial and noncoaxial deformation is compatible with transpression.

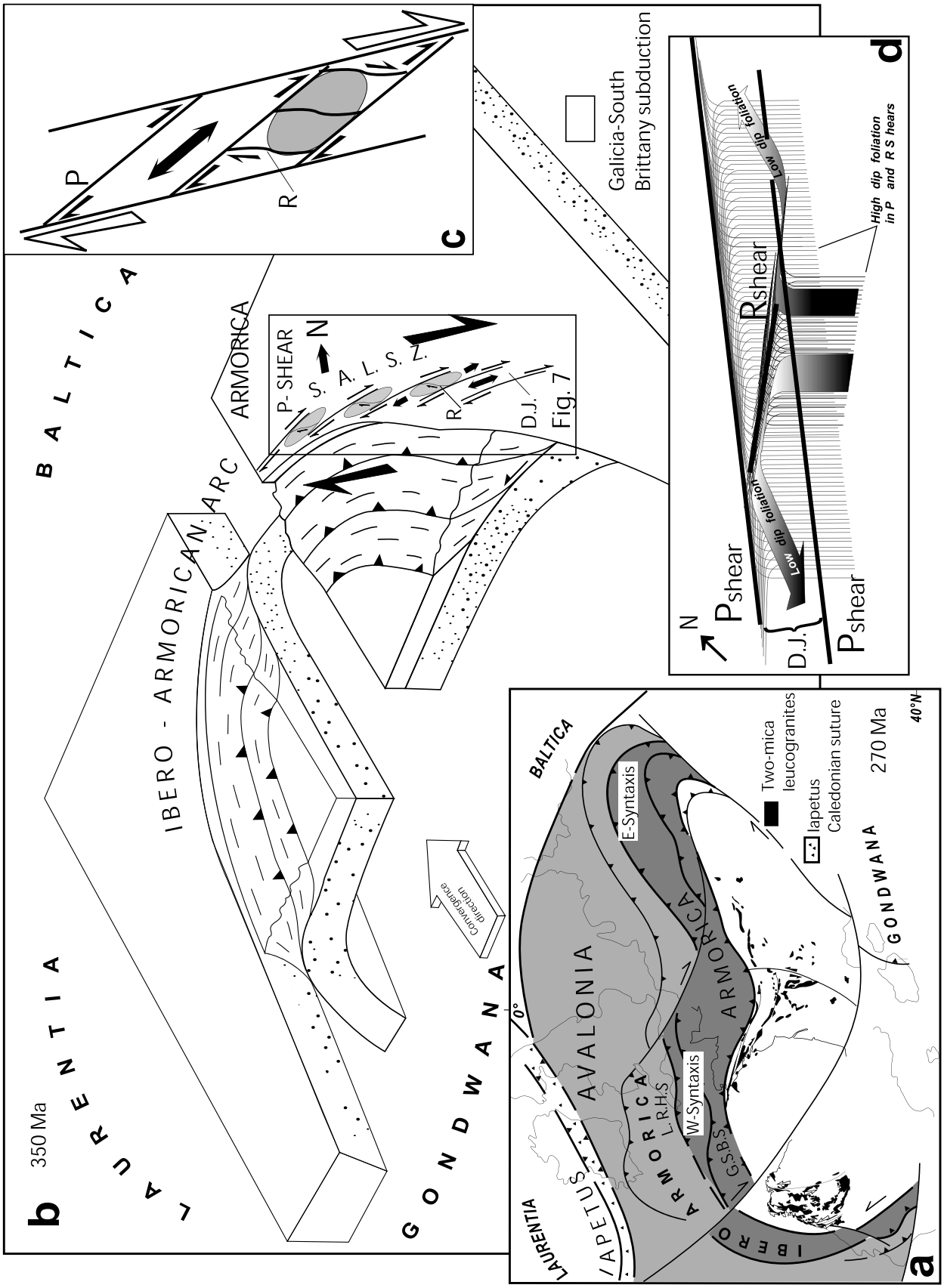
b
350 Ma
LAURENTIA
BALTICA
IBERO - ARMORICAN ARC
ARMORICA
P- SHEAR
S. A. L. S. Z.
N
R
D.J.
Fig. 7
GONDWANA
Convergence direction
c
P
R
Galicia-South Brittany subduction
d
N
Pshear
Rshear
Pshear
D.J.
Low dip foliation
Low dip foliation
High dip foliation in P and R S hears
a
LAURENTIA
IAPETUS
BALTICA
AVALONIA
ARMORICA
L.R.H.S
W-Syntaxis
E-Syntaxis
IBERO
GONDWANA
0°
40°N
270 Ma
Two-mica leucogranites
Iapetus
Caledonian suture

Figure 8

[56] It is worth noting that the syntectonic two-mica leucogranites record sinistral strike-slip shear at 340 Ma in the EMF and northward directed reverse shear at 325 Ma in the WMF. These varying ages, associated to different kinematic systems, infer a change of the kinematic framework between 340 and 325 Ma. Assuming a NW-SE convergence between Armorica and Gondwana plates (Figures 8a and 8b) [*Matte*, 1991], the dextral simple shear system evolves in time and induced a progressive clockwise rotation of structures during magma emplacement. The error $\sigma 1$ changed from a NW-SE orientation to a N-S to NE-SW direction inducing northward reverse movement along the WMF. Most of the Limousin two-mica leucogranites display NW-SE trending lineations [*Faure*, 1995, *Gébelin et al.*, 2006], parallel to the axial direction of millimeter to kilometer-scale postfolial upright folds [*Faure*, 1995] consistent with a NE-SW directed shortening. The same shortening direction is detected in the two-mica leucogranites on the NE edge of the Millevaches massif which recorded during their cooling southwest directed reverse faulting (see section 3.2). This mechanism that could be explained by the emplacement of the Millevaches granites, around 320 Ma, up against the Guéret granite already cooled by 335 Ma [*Faure et al.*, 2002], is in agreement with a transpressive setting [*Sanderson and Marchini*, 1984].

[57] The syntectonic two-mica leucogranites can provide further information in support to a transpressional tectonic setting. The Millevaches pluton, a representative example of Limousin syntectonic granites, displays a sigmoidal pattern of magnetic foliations and lineations consistent with right-lateral shear along the Pradines fault. Magnetic lineations rotate gradually from NNW-SSE in the center of the shear zone to NW-SE outside [*Gébelin et al.*, 2006]. In agreement with our $^{40}Ar/^{39}Ar$ and U-Pb data [*Gébelin*, 2004], such observations suggest that granite emplacement was contemporaneous with deformation along the Pradines shear zone. The Millevaches granites display horizontal lineations, both within and outside of shear bands that developed during bulk strike-slip-dominated transpression [*Gébelin et al.*, 2006]. This is consistent with a strike-slip-dominated transpressional setting, most likely occurring under low finite strain and/or with a small angle of convergence [*Tikoff and Greene*, 1997].

8.2. Magma Emplacement Hypothesis

[58] We propose that magma migrated along P shear and tension gashes formed in ductile shear zones, in a manner similar to the model proposed by *Tikoff and Teyssier* [1992] for the Sierra Nevada (Figure 8c). The main strike-slip shear zone, the ''South Armorican–Limousin Shear Zone'' (SALSZ), extends with a NW-SE trend from the South Armorican Massif to the Limousin region. Following the Variscan crustal thickening event related to the Galicia–south Brittany ocean northward subduction below the Armorica microplate (Figures 8a and 8b) [*Matte*, 2002], the large dextral simple SALSZ develops south and oblique to the suture (Figure 8b). En echelon P shears could develop at a low angle to the subduction trend with a sense of shear similar to that of the main shear zone (SALSZ, Figure 8b). The array of P shears provides a continuous dilational zone (dilational jogs or extensional duplexes [*Swanson*, 1988]) in the bridges between P shears in which magma may have been injected parallel to the direction of the P shears (Figures 8b and 8c). The P shears are connected by R-fracture-oriented shear zones (Figures 8b and 8c) that reduce the frictional resistance between two P shears [*Segall and Pollard*, 1980]. The Pradines fault could represent a R shear across the Ouzilly fault system. The magnetic foliations of Millevaches syntectonic granite are oriented NNW-SSE within the shear zone, over a 5 km width, and become subparallel to the inferred orientation of Ouzilly P shears [*Gébelin et al.*, 2006].

[59] Granites emplacement into dilational areas between P shears is consistent with the (1) NW-SE lineation trend and associated dextral shear bands observed in most Limousin granites [*Faure*, 1995, this study], (2) elongation of individual granites throughout the South Armorican Massif and the Limousin region, (3) orientation of the Pradines fault as an R shear connecting larger P shears, and (4) ''passive'' emplacement, consistent with the laccolith emplacement model described by *Gébelin et al.* [2006]. In this model, vertical shears may have helped to channel magmas from a deep source to their midcrustal emplacement level; then, magmas were trapped along discontinuities in the subhorizontal micaschist foliation acquired during the Variscan crustal thickening event. Within the P shears, granites should display steeply dipping foliations, whereas magma trapped between adjacent P shears, would migrate parallel to the P shears (Figure 8d, large black arrows) into the subhorizontal micaschist foliation. This would result in a 3-D laccolith shape, which has also been documented by gravimetric data [*Gébelin et al.*, 2004, 2006].

Figure 8. (a) Two-mica leucogranites current location on the possible configuration of the Variscan Belt of western Europe at 270 Ma, according to *Matte* [2002] modified. G.S.B.S., Galicia south Brittany Suture; L.R.H.S., Lizard Rheno Hercynian Suture. (b) Block diagram (according to *Matte* [1991], modified) showing a possible development of en echelon P shears at a low angle to the Galicia–south Brittany subduction trend with a sense of shear similar to that of the dextral South Armorican–Limousin Shear Zone (SALSZ); P, orientations of P shears; R, R shears; heavy arrow, direction of opening of tensional bridge; D.J., dilational jog. (c) Model of granite emplacement (gray ellipses) into tensional bridges (or dilational jogs, heavy arrow) between P shear proposed by *Tikoff and Teyssier* [1992] for the Sierra Nevada. (d) A 3-D model showing the relationship between P shears, R shears, and magma migration (heavy gray arrows) parallel to the direction of the P shears between two P shears (dilational jog). Granite will present a high-dip foliation within P shears and R shears while it will present a subhorizontal foliation in dilational jogs (D.J.) using the preexistent subhorizontal micaschists foliation during its migration.

[60] Steep foliations within shear zone and flat foliations outside shear zone are observed in other Limousin granites, in which the mode of emplacement could be similar to the Millevaches units. The synmagmatic leucogranites of the Marche fault [*Choukroune et al.*, 1983] display vertical foliation directly below the fault. The granite occurrence along the fault is emphasized by a high-gravity anomaly [*Dumas et al.*, 1990; *Gébelin et al.*, 2006], consistent with the interpretation of the Marche fault as a feeder zone. On both sides of the Marche fault, gravity modeling shows the occurrence of granite with a laccolith-like geometry rooted in the Marche fault. The Brâme granites present a laccolithic shape [*Audrain et al.*, 1989; *Gébelin et al.*, 2006] outside the Ouzilly strike-slip fault. In agreement with a previous AMS study [*Jover*, 1986] that reveals NW-SE magnetic lineations and flat foliations, the gravity results carried out on the Guéret biotite ± cordierite-bearing granites [*Gébelin et al.*, 2006] define a laccolith model of low thickness, but do not allow for the detection of the feeder zones. The Marche and Ouzilly synmagmatic faults (Figure 1) [*Lespinasse et al.*, 1986; *Mollier and Lespinasse*, 1985; this study] could represent P shear zones that drained magmas. The Limousin granites geometry emphasizes the clear genetic link between magmas emplacement and faults activity. The Limousin granites emplacement was clearly favored by shear zones activity, which has a large impact in the development of the internal magmatic fabric [*Jover*, 1986; *Gébelin et al.*, 2006]. The presence of mylonitized xenoliths into the fault zone, solid-state deformation following continuously from magmatic deformation [*Gébelin et al.*, 2006] and plutons not offset by shear zones represent evidences attesting to the shear zones control on magma emplacement. In the opposite of that *Neves et al.* [1996] suggested for some granites in the Borborema province, any evidences of magma emplacement predating strike-slip shearing and representing rheological heterogeneities that may induce strain localization and strike-slip shear zone nucleation, can be revealed in the Limousin region.

8.3. SALSZ: A Pop-up Structure

[61] We propose that the SALSZ in association with the array of P shears is a pop-up structure going from the South Armorican Massif to the Limousin region (Figure 9a). The association of P shears and pop-up structures has already been documented in similar transpressional zones, such as the San Andreas fault system [*Sylvester and Smith*, 1976; *Sylvester*, 1988; *Moore and Byerlee*, 1991]. In plane view, the ''pop-up structure'' is broadly lozenge-shaped, whereas in cross section it is bounded by convex-up faults that flatten toward the surface, forming a positive flower-palm tree structure [*Sylvester and Smith*, 1976; *Sylvester*, 1988; *McClay and Bonora*, 2001]. Any of vertical branches developing from the major shear zone forms a localization zone and a possible feeding zone for magmas. According to *McClay and Bonora* [2001], a pop-up asymmetry is generated when the boundary fault changes from strike-slip to oblique reverse-slip along strike. The Marche fault illustrates this switch, one that progressively evolved from sinistral strike-slip faulting to northward directed thrusting. In central Brittany, *Gumiaux et al.* [2004a] showed that the Champtoceaux Domain (Figure 7a) was affected during the Carboniferous by a bulk transpressional regime expressed by dextral strike-slip deformation and crustal-scale northward directed thrusting whose geometry and kinematics are consistent with a regional-scale NW-SE oriented dextral simple shear system.

[62] The rapid exhumation of Bt-Sil ± Cd gneisses at around 350 Ma may be explained in part by the pop-up structure activity. Indeed, strike-slip and reverse faults that are connected at depth to form a single fault system, would have been active at the same time (Figure 9a) allowing in a short period, thrusting, shearing, and exhumation. However, because the pop-up structure activity is probably not the only mechanism responsible of rocks exhumation this inference remains a question open for debate.

[63] On the basis of mantle tomography [*Gumiaux et al.*, 2004b] and seismic data [*Bitri et al.*, 2003], the South Armorican shear zone could have a lithospheric extension. The SALSZ appears as an important transcontinental structural object that can be compared to the largest Asian faults as the Red River fault [*Leloup et al.*, 1999] or to the transcurrent shear zone of Bororema region in NE Brazil [*Tommasi and Vauchez*, 1994].

9. Discussion in the Scope of the Geology of the French Massif Central

[64] The new field, microstructural, and Ar-Ar data on NW Massif Central provide constraints on the timing and tectonic setting of granite magmatism during the last stages of the Variscan orogeny. The new data support ascent and emplacement in a strike-slip regime which can be integrated with previous work in the Armorican Massif. The Armorican Massif is characterized, in Carboniferous times, by right-lateral strike-slip shear and synkinematic granite emplacement [*Berthé et al.*, 1979]. Along the southern Armorican shear zone, maximum shortening trends NE-SW, and vertical finite elongation is small, since deformation is close to simple shear [*Berthé et al.*, 1979]. These arguments and geochronologic similarities (section 7) suggest that the Armorican and Limousin regions formed a single large-scale shear zone, with the geometry of a pop-up/flower structure (SALSZ).

[65] Previous investigations [*Faure*, 1989; *Faure and Pons*, 1991; *Faure*, 1995] had, on the contrary, emphasized the role of late orogenic extension (Middle Carboniferous) in the emplacement of granite plutons in the Limousin region. This extension was thought to have been active from the late Visean in the Limousin, while compression dominated in the southernmost domains of the Montagne Noire and Pyrénées [*Faure*, 1995]. The evidence for the Middle Carboniferous extensional event, synchronous with the emplacement of the two-mica leucogranites, was based only on the geometry of the plutons, and on the NW-SE lineation recorded by the plutons. *Faure* [1995] describes ductile stretching along a NW-SE trend that occurred at the same time as NE-SW directed horizontal shortening; this shortening producing large-scale antiforms and synforms.

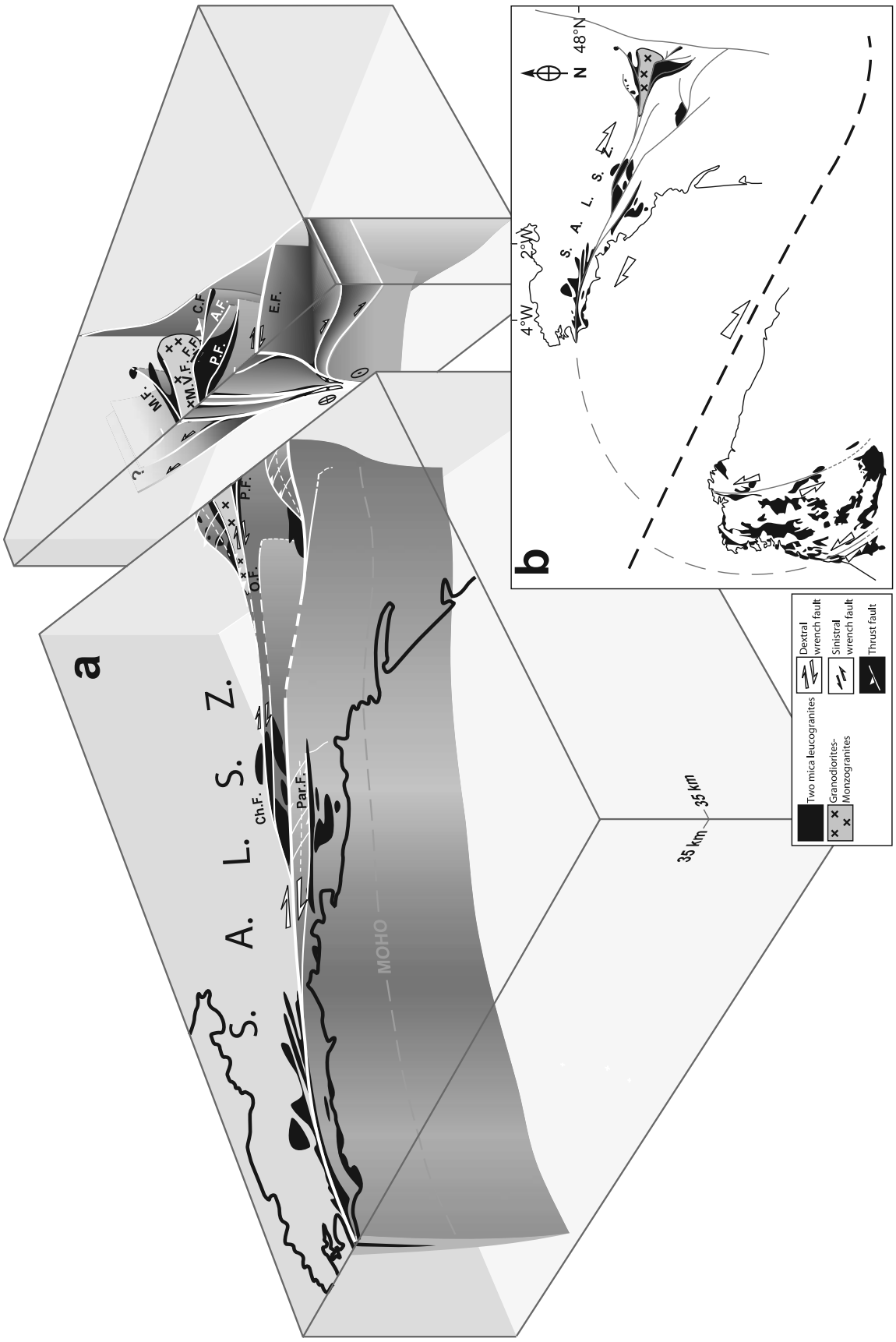

Figure 9. (a) Sketch of continental strike-slip faulting, illustrating the "pop-up structure" 3-D geometry around 300 Ma affecting the Armorican Massif and the Limousin area from 350 Ma. S.A.L.S.Z., South Armorican–Limousin Shear Zone; Ch.F., Cholet Fault; Par.F., Partenay Fault; M.F.: Marche Fault; O.F., Ouzilly Fault; M.V.F., St. Michel de Veisse Fault; P.F., Pradines Fault; A.F., Ambrugeat Fault; F.F., Felletin Fault; C.F., Courtine fault; E.F., Estivaux Fault. (b) Possible extension of the "pop-up structure" in Galicia.

These two finite strain directions are in agreement with the new data that are interpreted in terms of transpression, based on new structural, geophysical and geochronological data [this study, *Gébelin et al.*, 2004; *Gébelin*, 2004, *Gébelin et al.*, 2006]. It is worth noting that in the southernmost parts of the French Massif Central (Montagne Noire), kilometer-scale south verging recumbent folds developed in the late Visean–early Namurian [*Feist and Galtier*, 1985]. Evidence for shortening at this time is also reported in the Pyrénées [*Vissers*, 1992].

[66] However, the coexistence of a synmagmatic dextral strike-slip tectonics at 315 Ma in the Limousin, and the development of metamorphic core complexes (Velay dome and Montagne Noire) in other parts of the French Massif Central at the same period [*Burg and Vanderhaeghe*, 1993; *Ledru et al.*, 2001] remain to be explained? Indeed, migmatites associated with larger laccoliths of leucogranites dated at 314 ± 5 Ma and emplaced within the detachment zones [*Mougeot et al.*, 1997] are exhumed in the Velay. Also, the fact that the Montagne Noire dome displays similar characteristics to the Velay dome [*Van Den Driesche and Brun*, 1991] is puzzling. Several authors [*Burg and Matte*, 1978; *Mattauer et al.*, 1996; *Matte et al.*, 1998] related the geometry of the Montagne Noire to a large compressional anticline followed by nappe stacking. Other authors interpreted it as a result of orogenic collapse, due to gravitational instability after tectonic thickening [*Van Den Driesche and Brun*, 1991], assisted by strike-slip faulting [*Echtler and Malavieille*, 1990].

[67] The Brâme syntectonic leucogranites in the Limousin [*Mollier and Bouchez*, 1982; *Faure and Pons*, 1991; *Faure et al.*, 1990], emplaced at 324 ± 4 Ma (U-Pb on zircon [*Holliger et al.*, 1986]), may share some similarities with the leucogranites of the Velay dome. According to *Scaillet et al.* [1996a], these leucogranites record a progressive exhumation along N-S normal faults such as Nantiat fault to the west and BMF to the east (Figure 1), with cooling ages varying between 301 Ma at the base, 305 Ma in the center and 314 Ma at the top of the pluton. These cooling ages imply that the Brâme massif exhumation along the Nantiat and BMF normal faults is syn- to post-Millevaches massif deformation and emplacement at around 315 Ma [this study; *Gébelin*, 2004] in a dextral strike-slip setting.

[68] In agreement with other similar studies [e.g., *Vanderhaeghe and Teyssier*, 2001], the Nantiat and BMF normal faults, which are perpendicular to the usual E-W trend of the Variscan Belt, may be interpreted as synconvergent detachment faults that were active during gravity-driven flow. *Vanderhaeghe and Teyssier* [2001] show that the instantaneous and finite strain patterns observed in orogenic belts are not related to plate kinematics in a simple way but that gravity-driven flow plays a significant role in the deformation of thickened crust. They also show the importance of a layer of low-viscosity rocks in the middle crust that induces a mechanical decoupling between the subducting plate and the overlying thickened orogenic crust. According to *Vanderhaeghe and Teyssier* [2001], the first stage of synconvergent gravity-driven flow corresponds to widening of the continental plateau. At this stage, migration of the topographic front at the edges of the plateau, proceeds owing to the development of strike-slip faults, of which the SALSZ of the Ibero-Armorican arc could be an example (Figure 8a). The second stage of gravity-driven flow corresponds to the development of normal faults in the hinterland potentially compensated by compression and thrusting at the front of the sliding units [*Vanderhaeghe and Teyssier*, 2001]. This stage is also contemporaneous with the exhumation of low-viscosity partially molten crust in the hinterland of the orogen. As a part of the N-S striking Argentat ductile and brittle fault [*Lameyre*, 1984; *Ledru and Autran*, 1987; *Mattauer et al.*, 1988], which separates the Millevaches granites from the Limousin metamorphic units [*Floc'h*, 1983], the Brâme boundary normal faults (Nantiat and BMF, Figure 1) probably developed at the end of the dextral simple shear at circa 310–300 Ma. However, previous AMS and gravity studies suggest that the Argentat fault developed in the Millevaches pluton roof during its cooling, and not during the emplacement of the Millevaches pluton itself [*Gébelin et al.*, 2006].

[69] The Variscan Belt, may have developed a layer of low-viscosity rocks inducing mechanical decoupling between the subducting plate and the overlying thickened orogenic crust. This layer might have been exhumed as attested by granulitic-grade metamorphic rocks exposed in the Millevaches cooled from 315 Ma (U-Pb [*Gébelin*, 2004]) to circa 315–310 Ma ($^{40}Ar/^{39}Ar$ [this study]); ages which correspond also to the end of the SALSZ activity.

[70] Because of erosion and postkinematic dismantling of the Variscan Belt, it is difficult to piece together its evolution in detail. However, the new data set supports the hypothesis that granitic plutons were emplaced in a transpressive setting until 300 Ma and not in an extensional setting as previously thought.

10. Conclusion

[71] This structural, microstructural and geochronological study emphasizes the relationships between granite emplacement and ductile shear. The new $^{40}Ar/^{39}Ar$ age dates and microstructural data on mylonites in the Limousin area allow to estimate that dextral strike-slip faulting started circa 360–350 Ma and lasted until circa 300 Ma. Although the Variscan Belt is now deeply eroded and the evidence for plate kinematics has disappeared, many features (combination of coaxial and non-coaxial deformation, horizontal lineations within and outside of shear bands, etc.) observed within the Limousin granites suggest an emplacement in a transpressive setting. In this context, the emplacement of granitic plutons between an en echelon array of active P shears, associated with a strike-slip shear zone (SALSZ) slightly oblique to the Galicia–south Brittany ocean suture, appears to be one of the most favorable emplacement mechanism to explain (1) the current NW-SE elongation of the Limousin and Armorican Massif plutons (Figures 8a and 9a), (2) the orientation of the Pradines dextral strike-slip fault, as an R shear connecting larger P shears, and (3) the laccolithic shape of the Limousin and Armorican plutons.

[72] Indeed, in the Limousin and Armorican massifs, the two generations of granitoids (biotite ± cordierite-bearing granites and two-mica leucogranites) were probably associated with oblique convergence between the Laurentia-Baltica and Gondwana plates (Figure 8b). Assuming NW-SE convergence between the Armorica and Gondwana plates [*Matte*, 1991], we propose that following the Variscan crustal thickening event, at around 360–350 Ma [*Matte*, 2002], an array of en echelon P shears developed with a SW-NE to WSW-ENE trend, at a low angle to the subduction, over a distance of at least 300 km in the southeastern portion of the western syntaxis of the Variscan Belt (Figures 8a and 8b). The dextral simple shear system evolving in time induced a progressive clockwise rotation of structures to their current NW-SE position. The onset of shearing is constrained by the biotites of the Bt-Sil ± Cd gneisses that reveal an age of circa 350 Ma, postdating the high-temperature strike-slip deformation.

[73] The array of P shears is associated with the SALSZ, probably of lithospheric scale (based on mantle tomography [*Gumiaux et al.*, 2004b] and seismic data [*Bitri et al.*, 2003]), going from the South Armorican Massif to the Limousin. In agreement with previous work [*Sylvester and Smith*, 1976; *Sylvester*, 1988] in transpressive settings, we compare this large shear zone to a ''pop-up'' structure'', now partially eroded. Strike-slip and reverse faults that are connected at depth to form a single fault system are activated at the same time and may explain in part the rapid exhumation of Bt-Sil ± Cd gneisses at circa 350 Ma.

[74] Thus the Limousin and Armorican massifs can be described as ductile, right-lateral, strike-slip ''pop-up'' zones within which granitic magmas were channeled and deformed from 350 Ma to 300 Ma. The Guéret biotite-bearing granites that were emplaced at 350 Ma [*Berthier et al.*, 1979] have recorded the Ouzilly dextral strike-slip shear zone movement during their cooling between 700°C and 400°C. The end of lateral shear is recorded within shear bands of ultramylonitic two-mica leucogranites, but also by the observation of Stephanian sedimentary formations sheared into the SASZ [*Rolin and Colchen*, 2001]. In this model, P shears channel the magmas at depth, inducing a high-dip foliation in the granites, while between two P shears, magmas were trapped and migrate into the subhorizontal micaschist host rock (Figure 8d), one that has a subhorizontal foliation, inducing a 3-D laccolithic shape (revealed by gravimetric data [*Gébelin et al.*, 2004, 2006]). This mode of emplacement could explain why the large outcropping surface of granites at this erosion level, is at variance with their real thickness and abundance in the crust.

[75] The N-S striking normal faults, perpendicular to the usual E-W trend of the Variscan Belt, that developed at the end of the strike-slip faulting and that probably played a significant role in the exhumation of the two-mica leucogranites [*Scaillet et al.*, 1996a], could be interpreted as synconvergent normal faults that developed during gravity-driven flow [*Vanderhaeghe and Teyssier*, 2001]. This event is contemporaneous with local exhumation of ductile crust represented by the Millevaches granulites, at circa 315 Ma ($^{40}Ar/^{39}Ar$ [this study] and U-Pb method [*Gébelin*, 2004]).

[76] The Galician region, along the western end of the Ibero-Armorican tectonic arc (Figures 8a and 9b), exhibits major left-lateral ductile shear zones, also associated with voluminous granite magmatism dated between 330 and 310 Ma [*Fernandez-Suarez et al.*, 2000; *Valle Aguado et al.*, 2005]. The Galician shear zones can be interpreted as conjugate and mirror structures to the Limousin and Armorican shear zones (Figure 9b), developed from the first stage of synconvergent gravity-driven flow of the Variscan belt.

Appendix A: Electron Backscatter Diffraction Method and Analytical Procedure

[77] Quartz preferred orientations were measured by using scanning electron backscatter diffraction techniques (EBSD [*Lloyd et al.*, 1991; *Adams et al.*, 1993; *Dingley and Field*, 1997]) on the EBSD/SEM system at ISTEEM Montpellier. Backscattered electron (BSE) diffraction on the scanning electron microscope has become an important tool for the combined study of microstructures in crystalline materials. It is possible to measure complete crystallographic orientations of single crystallites with direct reference to the microstructure [*Neumann*, 2000; *Heidelbach et al.*, 2000].

[78] EBSD is based on the automatic analysis of diffraction patterns. These patterns, composed of Kikuchi bands, are generated by the interaction of a vertical incident electron beam with a flat crystal surface. A phosphor screen is located close to the thin section to collect the backscattered electrons and to emit a photonic image, which is then processed and indexed using the CHANNEL+software [*Schmidt and Olesen*, 1989]. The Euler angles ($\varphi1$, $\varphi2$, $\varphi3$) are determined for each quartz grain and stored with the nature of the mineral. The whole procedure can be carried out automatically. The precision of crystal orientations measured from electron backscattering patterns is better than 1° [*Krieger Lassen*, 1996].

Appendix B: The $^{40}Ar/^{39}Ar$ Dating

B1. Analytical Procedure for Bulk Samples

[79] The bulk samples of biotite and muscovite were separated by magnetic separators and sometimes by heavy liquids. All of the final mineral separates were obtained by hand-picking. The samples were irradiated in the McMaster University (Hamilton, Ontario, Canada) reactor with total fluxes of 10^{18} n/cm^2. The irradiation standard is the Fish Canyon Tuff sanidine (28.48 Ma [*Schmitz and Bowring*, 2001; *Schmitz et al.*, 2003]).

[80] The classical step heating procedure, used for bulk samples, is described by *Arnaud et al.* [1993, 2003]. Heating was performed using a double vacuum furnace allowing for a good thermal resolution during the fractionated degassing process. After extraction and purification of rare gases on active alloy getters, argon was introduced in a

VG 3600 mass spectrometer and isotopes from mass 36 to mass 40 were measured by peak-switching in six runs. Ages have been calculated after correction for blanks (varying between 2.240×10^{-14} cm^3 and 3.36×10^{-12} cm^3 for ^{40}Ar and between 1.344×10^{-14} cm^3 and 4.48×10^{-15} cm^3 for ^{36}Ar), mass discrimination, radioactive decay of ^{39}Ar and ^{37}Ar, and irradiation-induced mass interferences. Errors are given at 1σ.

B2. Analytical Procedure for Single Grains

[81] The single grains of biotite and muscovite for the laser probe experiments were carefully selected under a binocular microscope from a coarse fraction of the crushed rock sample. They were then ultrasonically cleaned in methanol and distilled water to remove surface related contaminants such as small feldspar grains. All samples were packed in aluminum foil and irradiated for 70 hours in the McMaster nuclear reactor together with the MMHb4 hornblende neutron flux monitor dated at 520.4 ± 1.7 Ma. After irradiation, all samples were placed on a Cu holder inside a UHV gas extraction system and baked for 48 hours at 200°C. Step heating of single grain, spot fusion, and polished section were conducted with the laser operating in the continuous or semipulsed mode [*Monié et al.*, 1997]. The analytical device consists of: a multiline continuous 6-W argon ion laser; a beam shutter for selection of exposure times; divergent and convergent lenses for definition of the beam diameter; a small inlet line for the extraction and purification of gases; and a MAP 215-50 noble gas mass spectrometer. For the laser spot fusions done on a single crystal or on a polished section, the maximum laser beam diameter was 50 μm for 20 to 40 μm in depth. The experiments are monitored through a binocular microscope coupled with a video color camera to observe the mineral behavior during laser probe degassing. Each analysis involves 5 min for gas extraction and cleaning and 15 min for data acquisition by peak switching from mass 40 to mass 36. System blanks were evaluated every three analyses and ranged from 3×10^{-12} cm^3 for ^{40}Ar to 4×10^{-14} cm^3 for ^{36}Ar. Ages and errors were calculated according to *McDougall and Harrison* [1999]. Errors are given at 1 sigma. The error on the irradiation J factor was only considered in the calculation of total gas ages, plateau ages and intercept ages in the isotope correlation plots. For spot fusion experiments on single grains, the mean age was obtained by cumulating the amount of argon isotopes released at each experiment (as for a total age). The error was obtained by propagation of errors during the various steps of age calculation.

[82] **Acknowledgments.** This work has been supported by the BRGM as part of the French geological map program. We would like to thank P. Rossi, M. De St Blanquat, P. Matte, and M. Mattauer for fruitful discussions concerning granite emplacement as well as on the Variscan Belt geology. D. Marquer and P. Rolin are thanked for sharing their knowledge of the Limousin geology. A. Tommasi is warmly thanked for helping with the EBSD results and A. Delplanque for providing support in the 3-D drawing. We are also greatly indebted to C. Nevado for preparing our polished thin rock sections. Special thanks go to E. C. Ferré for his helpful comments resulting in significant improvements. The authors wish to thank very much O. Vanderhaeghe and P. Rey for constructive comments that helped to greatly improve the manuscript and Matthew Downey for English editing.

References

Adams, B. I., S. I. Wright, and K. Kunze (1993), Orientation imaging: The emergence of a new microscopy, *Metall. Trans. A*, *24*, 819–831.

Alexandrov, P., A. Cheilletz, E. Deloule, and M. Cuney (2000), 319 ± 7 Ma age for the Blond granite (northwest Limousin, French Massif Central) obtained by U-Pb ion-probe dating of zircons, *C. R. Acad. Sci.*, *330*, 1–7.

Arnaud, N., M. Brunel, J. M. Cantagrel, and P. Tapponnier (1993), High cooling and denudation rates at Kongur Shan, eastern Pamir (Xinjiang, China) revealed by ^{40}Ar/^{39}Ar alkali feldspar thermochronology, *Tectonics*, *12*, 1335–1346.

Arnaud, N., P. Tapponnier, F. Roger, M. Brunel, U. Scharer, C. Wen, and X. Zhiqin (2003), Evidence for Mesozoic shear along the western Kunlun and Altyn-Tagh fault, northern Tibet (China), *J. Geophys. Res.*, *108*(B1), 2053, doi:10.1029/2001JB000904.

Audrain, J., J. L. Vigneresse, M. Cuney, and M. Friedrich (1989), Modèle gravimétrique et mise en place du complexe granitique hyperalumineux de St Sylvestre (Massif Central Français), *C. R. Acad Sci., Ser. 2*, *309*, 1907–1914.

Autran, J., and J. Lameyre (1980), Evolutions géologiques de la France, *Mem. BRGM*, *107*, 87–97.

Bernard-Griffiths, J., J.-J. Peucat, S. Sheppart, and P. Vidal (1985), Petrogenesis of Hercynian leucogranites from the southern Armorican Massif: Contribution of REE and isotopic (Sr, Nb, Pb and O) geochemical data to the study of source rock characteristics and ages, *Earth Planet. Sci. Lett.*, *74*, 235–250.

Berthé, D., P. Choukroune, and P. Jegouzo (1979), Orthogneiss, mylonite and non-coaxial deformation of granites: The example of the South Armorican shear zone, *J. Struct. Geol.*, *1*, 31–42.

Berthier, F., J. L. Duthou, and M. Roques (1979), Datation géochronologique Rb/Sr sur roches totales du granite de Guéret (Massif Central). Age fini-Dévonien de mise en place de l'un de ses faciès types, *Bull. Bur. Rech. Geol. Min. Fr.*, *1*, 31–42.

Bertrand, J. M., J. Leterrier, M. Cuney, M. Brouand, J. M. Stussi, E. Delaperierre, and D. Virlogieux (2001), Géochronologie U-Pb sur zircons de granitõuml;des du Confolentais, du massif de Charroux-Civray (seuil du Poitou) et de Vendée, *Geol. Fr.*, *1–2*, 167–181.

Bitri, A., M. Ballèvre, J. P. Brun, J. Chantraine, D. Gapais, P. Guennoc, C. Gumiaux, and C. Truffert (2003), Imagerie sismique de la zone de collision hercynienne dans le Sud-Est du Massif armoricain (projet Armor 2/programme Géofrance 3D), *C. R. Geosci.*, *335*, 969–979.

Bouchez, J.-L., and O. Jover (1986), Le Massif Central: Un chevauchement de type himalayen vers l'ouest-nord-ouest, *C. R. Acad. Sci., Ser. II*, *302*, 675–680.

Boutin, R., and R. Montigny (1993), Datation ^{39}Ar/^{40}Ar des amphibolites du complexe leptyno-amphibolique du plateau d'Aigurande: Collision varisque à 390 Ma dans le Nord-Ouest du Massif Central Français, *C. R. Acad. Sci., Ser.2*, *316*, 1391–1398.

Burg, J.-P., and P. Matte (1978), A cross-section through the French Massif Central and the scope of its Variscan geodynamic evolution, *Z. Dtsch. Geol. Ges.*, *139*, 429–460.

Burg, J.-P., and O. Vanderhaeghe (1993), Structures and way-up criteria in migmatites, with application to the Velay dome (French Massif Central), *J. Struct. Geol.*, *15*(11), 1293–1301.

Burg, J.-P., A. Leyreloup, J. Marchand, and P. Matte (1984), Inverted metamorphic zonation and large scale thrusting in Variscan Belt: An example in the French Massif central, in *Variscan Tectonics of the North Atlantic Region*, edited by D. H. W. Hutton and D. J. Sanderson, *Geol. Soc. Spec. Publ.*, 44–61.

Burg, J.-P., J. P. Brun, and J. Van Den Driesche (1990), Le sillon houiller du Massif Central Français: Faille de transfert pendant l'amincissement crustal de la chaine varisque?, *C. R. Acad. Sci., Ser.*, *311*, 147–152.

Choukroune, P., D. Gapais, and P. Matte (1983), Tectonique hercynienne et deformation cisaillante: La faille ductile senestre de la Marche (Massif Central Français), *C. R. Acad. Sci.*, *296*, 859–862.

Copeland, P., R. R. Parrish, and T. M. Harrison (1988), Identification of inherited Pb in monazite and its implications for U-Pb systematics, *Nature*, *333*, 760–763.

Costa, S., and P. Rey (1995), Lower crustal rejuvenation and crustal growth during post-thickening collapse: Insights from a crustal cross section through a metamorphic core complex, *Geology*, *23*, 905–908.

Costa, S., H. Maluski, and J. M. Lardeaux (1993), ^{40}Ar-^{39}Ar chronology of Variscan tectonometa-

morphic events in an exhumed crustal nappe: The Monts du Lyonnais complex (Massif Central, France), *Chem. Geol.*, *105*, 339–359.

Cuney, M., M. Friedrich, P. Blumenfeld, A. Bourguignon, M. C. Boiron, J. L. Vigneresse, and B. Poty (1990), Metallogenesis in the French part of the Variscan orogen. Part I: U preconcentrations in pre-Variscan and Variscan formations: A comparison with Sn, W and Au, *Tectonophysics*, *177*, 39–57.

Cuney, M., M. Brouand, and J. M. Stussi (2001), Le magmatisme hercynien en Vendée. Corrélations avec la socle du Poitou et l'ouest du Massif Central Français, *Geol. Fr.*, nos. 1–2, 117–142.

Dahl, P. S. (1996), The effect of composition on retentivity of argon and oxygen in hornblende and related amphiboles: A field-tested empirical model, *Geochim. Cosmochim. Acta*, *60*, 3687–3700.

Davidson, C., L. S. Hollister, and S. M. Schmid (1992), Role of melt in the formation of a deep-crustal compressive shear zone: The MacLaren Glacier metamorphic belt, South Central Alaska, *Tectonics*, *11*, 348–359.

Davidson, C., S. M. Schmid, and L. S. Hollister (1994), Role of melt during deformation in the deep crust, *Terra Nova*, *6*, 133–142.

Dingley, D. J., and D. P. Field (1997), Electron backscatter diffraction and orientation imaging microscopy, *Mater. Sci. Technol.*, *13*(1), 69–78.

Downes, H., and J.-L. Duthou (1988), Isotopic and trace-element arguments for the lower-crustal origin of Hercynian granitoids and pre-Hercynian orthogneisses, Massif Central (France), *Chem. Geol.*, *68*, 291–308.

Dumas, E., M. Faure, and J. Pons (1990), L'architecture des plutons leucogranitiques du plateau d'Aigurande et l'amincissement crustal tardi-varisque, *C. R. Acad. Sci., Ser. 2*, *310*, 1533–1539.

Duthou, J.-L. (1977), Chronologie Rb-Sr et géochimie des granitoïdes d'un segment de la chaîne varisque. Relations avec le métamorphisme: Le Nord-Limousin, thèse 3ème cycle, 290 pp., Univ. de Clermont-Ferrand Clermont-Ferrand France.

Duthou, J. L., J. M. Cantagrel, J. Didier, and Y. Vialette (1984), Palaeozoic granitoids from the French Massif Central: Age and origin studied by ^{87}Rb-^{87}Sr system, *Phys. Earth Planet. Inter.*, *35*, 131–144.

Duthou, J. L., M. Chenevoy, and M. Gay (1994), Age Rb-Sr Dévonien moyen des migmatites à cordierite des Monts du Lyonnais (Massif Central Français), *C. R. Acad. Sci., Ser. II*, *319*, 791–796.

Echtler, H., and J. Malavieille (1990), Extensional tectonics, basement uplift and Stephano-Permian collapse basin in a Late Variscan metamorphic core complex (Montagne Noire, southern Massif Central), *Tectonophysics*, *177*, 125–138.

Faure, M. (1989), L'amincissement crustal de la chãcirc;ne varisque à partir de la déformation ductile des leucogranites du Limousin, *C. R. Acad. Sci., Ser. II*, *309*, 1839–1845.

Faure, M. (1995), Late carboniferous extension in the Variscan French Massif Central, *Tectonics*, *14*, 132–153.

Faure, M., and J. Pons (1991), Crustal thinning recorded by the shape of the Namurian-Wesphalian leucogranite in the Variscan Belt of the northwest Massif Central, France, *Geology*, *19*, 730–733.

Faure, M., A. Prost, and E. Lasne (1990), Déformation ductile extensive d'âge Namuro-Wesphalien dans le plateau d'Aigurande, Massif Central Français, *Bull. Soc. Geol. Fr.*, *8*, 189–197.

Faure, M., C. Leloix, and J.-Y. Roig (1997), L'évolution polycyclique de la chãcirc;ne hercynienne, *Bull. Soc. Geol. Fr.*, *168*, 695–705.

Faure, M., P. Monié, C. Pin, H. Maluski, and C. Leloix (2002), Late Visean thermal event in the northern part of the French Massif Central: New ^{40}Ar/^{39}Ar and Rb-Sr isotopic constraints on the Hercynian syn-orogenic extension, *Int. J. Earth Sci.*, *91*, 53–75.

Feist, R., and J. Galtier (1985), Découverte de flores d'âge namurien probable dans le flysch à olistolithes de Cabrières (Hérault): Implications sur la durée de la sédimentation synorogénique dans la Montagne Noire (France méridionale), *C. R. Acad. Sci., Ser. 2*, *300*, 207–212.

Fernandez-Suarez, J., G. R. Dunning, G. A. Jenner, and G. Gutierrez-Alonso (2000), Variscan collisional magmatism and deformation in NW Iberia: Constraints from U-Pb geochronology of granitoids, *J. Geol. Soc. London*, *157*, 565–576.

Floc'h, J. P. (1983), La série métamorphique du Limousin central: Une traverse de la branche ligérienne de l'orogène varisque, de l'Aquitaine à la zone broyée d'Argentat (Massif Central Français), thèse d'Etat, 445 pp., Univ. Limoges, Limoges, France.

Freiberger, R., L. Hecht, M. Cuney, and G. Morteani (2001), Secondary Ca-Al silicates from Mid-European Hercynian granitoids: Implication for the cooling history of granitic plutons, *Contrib. Mineral. Petrol.*, *141*, 415–429.

Gardien, V. (1990), Reliques de grenat et de staurotide dans la série métamorphique de basse pression du Mont Pilat (Massif Central Français): Témoins d'une evolution tectono-métamorphique polyphasée, *C. R. Acad. Sci. Fr., Ser. II*, *310*, 233–240.

Gardien, V., J. M. Lardeaux, and M. Misseri (1988), Les péridotites des Monts du Lyonnais (MCF): Témoins privilégiés d'une subduction de lithosphère paléozõuml;que, *C. R. Acad. Sci.*, *307*, 1967–1972.

Gébelin, A. (2004), Déformation et mise en place des granites (360–300Ma) dans un segment de la Chãcirc;ne Varisque (Plateau de Millevaches, Massif Central), thèse, Univ. Montpellier, Montpellier, France.

Gébelin, A., G. Martelet, M. Brunel, M. Faure, and P. Rossi (2004), Late Hercynian leucogranites modelling as deduced from new gravity data: The example of the Millevaches massif, Massif Central, France, *Bull. Soc. Geol. Fr.*, *3*, *175*, 239–248.

Gébelin, A., G. Martelet, Y. Chen, M. Brunel, and M. Faure (2006), Structure of late Variscan Millevaches leucogranite massif in the French Massif Central: AMS and gravity modelling results, *J. Struct. Geol.*, *28*, 148–169.

Grolier, J. (1971), Contribution à l'étude géologique des séries cristallophylliennes inverses du Massif Central Français: La série de la Sioule (Puy de Dôme, Allier), *Mem. BRGM*, *64*, 163 pp.

Grolier, J., and J. Letourneur (1968), L'évolution tectonique du grand Sillon Houiller du Massif Central Français, *Proc. Int. Geol. Congr.*, *23rd*(I), 107–116.

Gumiaux, C., D. Gapais, J. P. Brun, J. Chantraine, and G. Ruffet (2004a), Tectonic history of the Variscan Armorican Shear belt (Brittany, France), *Geodin. Acta*, *17*(4), 289–307.

Gumiaux, C., S. Judenherc, J. P. Brun, D. Gapais, M. Granet, and G. Poupinet (2004b), Restoration of lithosphere-scale wrenching from integrated structural and tomographic data (Hercynian belt of western France), *Geol. Soc. Am.*, *32*(4), 333–336, doi:10.1130/G20134.2.

Hames, W. E., and S. A. Bowring (1994), An empirical evaluation of the argon diffusion geometry in muscovite, *Earth Planet. Sci. Lett.*, *124*, 161–169.

Harrison, T. M., I. Duncan, and Mc Dougall (1985), Diffusion of ^{40}Ar in biotite: Temperature, pressure and compositional effects, *Geochim. Cosmochim. Acta*, *49*, 2461–2468.

Heidelbach, F., K. Kunze, and H. R. Wenk (2000), Texture analysis of a recrystallised quartzite using electron diffraction in the scanning electron microscope, *J. Struct. Geol.*, *22*, 91–104.

Holliger, P., M. Cuney, M. Friedrich, and L. Turpin (1986), Age carbonifère de l'Unité de Brâme du complexe granitique perlumineux de St Sylvestre (NW du Massif Central) défini par les données isotopiques U-Pb sur zircon et monazite, *C. R. Acad. Sci., Ser. 2*, *303*, 1309–1314.

Hutton, D. H. W., and R. J. Reavy (1992), Strike-slip tectonics and granite petrogenesis, *Tectonics*, *11*, 960–967.

Jégouzo, P., and E. A. Rosello (1988), La branche Nord du cisaillement sud Armoricain (France): Un essai d'évaluation du déplacement par l'analyse des mylonites, *C. R. Acad. Sci., Ser. II*, *307*(17), 1825–1831.

Jover, O. (1986), Les massifs granitiques de Guéret et du nord-Millevaches. Analyse structurale et modèle de mise en place (Massif Central Français), thèse de doctorat, 233 pp., Univ. of Nantes, Nantes, France.

Jover, O., and J.-L. Bouchez (1986), Mise en place syntectonique des granitõuml;des de l'Ouest du Massif Central Français, *C. R. Acad. Sci., Ser. II*, *303*, 969–974.

Krieger Lassen, N. C. (1996), The relative precision of crystal orientations measured from electron backscattering patterns, *Microscopy, J.*, *181*, 72–81.

Kruhl, J. H., and M. Peternell (2002), The equilibration of high-angle grain boundaries in dynamically recrystallized quartz: The effect of crystallography and temperature, *J. Struct. Geol.*, *24*, 1125–1137.

Lafon, J. M., and J. P. Respaut (1988), Géochronologie U-Pb et leucogranites varisques: Cas des massifs de Grand-Rieu et de la Porcherie (Limousin), Massif Central Français, *Bull. Mineral.*, *111*, 225–237.

Lameyre, J. (1982), Contribution à la géologie du Limousin: Arguments pour des fenêtres ouvertes dans un grand charriage par des diapirs leucogranitiques, *C. R. Acad. Sci.*, *294*, 1237–1240.

Lameyre, J. (1984), Contribution à la géologie du Limousin; (II), Les leucogranites fini-carboniferes et le modele himalayen. Contribution to the geology of Limousin, France; (II), The Upper Carboniferous leucogranites and the Himalayan model, *C. R. Acad. Sci.*, *298*, 895–900.

Lardeaux, J.-M., P. Ledru, I. Daniel, and S. Duchene (2001), The Variscan French Massif Central: A new addition to the ultra-high pressure metamorphic 'club': Exhumation processes and geodynamic consequences, *Tectonophysics*, *332*, 143–167.

Launeau, P., J.-L. Bouchez, and P. Blumenfeld (1988), Structuration magmatique horizontale SE-NW du leucogranite de Crozant (Marche, Massif Central Français), *C. R. Acad. Sci., Ser. II*, *307*, 295–302.

Le Breton, N., and A. B. Thompson (1988), Fluid-absent (dehydration) melting of biotite in metapelites in the early stages of crustal anatexis, *Contrib. Mineral. Petrol.*, *99*, 226–237.

Le Carlier de Veslud, C., P. Alexandre, M. Cuney, G. Ruffet, A. Cheilletz, and D. Virlogeux (2004), Thermochronology ^{40}Ar/^{39}Ar et évolution thermique des granitõuml;des méso-varisques du complexe plutonique de Charroux-Civray (Seuil du Poitou), *Bull. Soc. Geol. Fr., Ser. 2*, *175*, 95–106.

Ledru, P., and A. Autran (1987), L'édification de la chãcirc;ne varisque dans le Limousin. Rôle de la faille d'Argentat à la limite Limousin-Millevaches, *Doc. BRGM*, *140*, 51–81.

Ledru, P., J.-M. Lardeaux, D. Santallier, A. Autran, J.-M. Quenardel, J.-P. Floc'h, G. Lerouge, N. Maillet, J. Marchand, and A. Ploquin (1989), Où sont les nappes dans le Massif Central Français?, *Bull. Soc. Geol. Fr.*, *8*, 605–618.

Ledru, P., A. Autran, and D. Santallier (1994a), Lithostratigraphy of Variscan terranes in the French Massif Central: A basis for paleogeographical reconstitution, in *Pre-Mesozoic Geology in France and Related Areas*, edited by J. D. Keppie, pp. 276–288, Springer, New York.

Ledru, P., S. Costa, and H. Echtler (1994b), The Massif Central: Structure, in *Pre-Mesozoic Geology in France and Related Areas*, edited by J. D. Keppie, pp. 305–323, Springer, New York.

Ledru, P., G. Courrioux, C. Dallain, J.-M. Lardeaux, J.-M. Montel, O. Vanderhaeghe, and G. Vitel (2001), Partial melting and flow of the Variscan orogenic crust: Anatomy of the Velay dome, French Central Massif, *Tectonophysics*, *342*, 207–237.

Leloup, P. H., Y. Ricard, J. Battaglia, and R. Lacassin (1999), Shear heating in continental strike-slip shear zones: Model and field examples, *Geophys. J. Int.*, *136*, 19–40.

Lerouge, G. (1988), Tectonogenèse compare de deux segments de la chãcirc;ne hercynienne: Le Massif Central Français septentrional et le sud du Massif

Armoricain, *Mem. Geodiff. 2*, 363 pp., Univ. Paris-Sud, Orsay, France.

Lespinasse, M., B. Mollier, J. Delair, and Y. Bladier (1986), Structuration tangentielle et chevauchements carbonifères dans les leucogranites du NW du Massif Central Français: L'exemple des failles de Bussières-Madeleine et d'Arrênes-Ouzilly, *C. R. Acad. Sci.*, *303*, 1575–1579.

Lloyd, G. E., N. H. Schmidt, D. Mainprice, and D. J. Prior (1991), Crystallographic textures, *Mineral. Mag.*, *55*, 331–345.

Mainprice, D. H., and M. S. Paterson (1984), Experimental studies on the role of water in the plasticity of quartzites, *J. Geophys. Res.*, *89*, 4257–4269.

Mattauer, M., M. Brunel, and P. Matte (1988), Failles normales ductiles et grands chevauchements: Une nouvelle analogie entre l'Himalaya et la chãcirc;ne hercynienne du Massif Central Français, *C. R. Acad. Sci., Ser. 2*, *306*, 671–676.

Mattauer, M., P. Laurent, and P. Matte (1996), Plissement hercynien synschisteux post-nappe et étirement subhorizontal dans le versant sud de la Montagne noire (Sud du Massif central, France), *C. R. Acad. Sci., Ser. IIa*, *322*, 309–315.

Matte, P. (1986), Tectonics and plate Tectonics model for the Variscan Belt of Europe, *Tectonophysics*, *126*, 329–374.

Matte, P. (1991), Accretionary history and crustal evolution of the Variscan Belt in western Europe, *Tectonophysics*, *196*, 309–339.

Matte, P. (2002), Variscides between the Appalachians and the Urals: Similarities and differences between Paleozoic subduction and collision belts, *Mem. Geol. Soc. Am.*, *364*, 239–251.

Matte, P., J. Lancelot, and M. Mattauer (1998), La zone axiale hercynienne de la Montagne noire n'est pas un metamorphic core complex extensive mais un anticlinal post-nappe à Coeur anatectique, *Geodin. Acta*, *11*, 13–22.

McClay, K., and M. Bonora (2001), Analog models of restraining stopovers in strike-slip fault systems, *AAPG Bulletin*, *85*, 233–260.

McDougall, I., and T. M. Harrison (1999), *Geochronology and Thermochronology by the $^{40}Ar/^{39}Ar$ Method*, 212 pp., Oxford Univ. Press, New York.

Ménard, G., and P. Molnar (1988), Collapse of a Hercynian Tibetan Plateau into a late Paleozoic European Basin and Range province, *Nature*, *334*, 235–237.

Mercier, L., J.-M. Lardeaux, and P. Davy (1991), On the tectonic significance of retrograde P-T-t paths in eclogites of the French Massif Central, *Tectonics*, *10*, 131–140.

Mercier, L., V. Johan, J.-M. Lardeaux, and P. Ledru (1992), Evolutions tectono-métamorphiques des nappes de l'Artense (Massif Central Français): Nouveaux marqueurs de la collision dans la chãcirc;ne varisque, *Bull. Soc. Geol. Fr.*, *163*, 641–649.

Mollier, B., and J. L. Bouchez (1982), Structuration magmatique du complexe granitique de Brâme-St Sylvestre-St Goussaud (Limousin, Massif Central Français), *C. R. Acad. Sci., Ser. 2*, *294*, 1329–1334.

Mollier, B., and M. Lespinasse (1985), Déformation magmatique et plastique en limite Nord du granite de Saint-Sylvestre (Nord-Ouest du Massif Central Français): La faille d'Arrênes-Ouzilly, *C. R. Acad. Sci.*, *300*, 681–686.

Monié, P., R. Caby, and M. H. Arthaud (1997), The Neoproterozoic brasiliano orogen of northeast Brazil.^{40}Ar-^{39}Ar ages and petro-structural data from Ceara, *Precambrian Res.*, *81*, 241–264.

Moore, D. E., and J. D. Byerlee (1991), Comparative geometry of the San Andreas fault, California, and laboratory fault zones, *Geol. Soc. Am. Bull.*, *103*, 762–774.

Mougeot, R., J.-P. Respaut, P. Ledru, and C. Marignac (1997), U-Pb chronology on accessory minerals of the Velay anatectic dome (French Massif Central), *Eur. J. Miner.*, *9*, 141–156.

Neumann, B. (2000), Texture development of recrystallised quartz polycrystals unravelled by orientation and misorientation characteristics, *J. Struct. Geol.*, *22*, 1695–1711.

Neves, S. P., A. Vauchez, and C. J. Archanjo (1996), Shear zone-controlled magma emplacement or magma-assisted nucleation of shear zones? Insights from northeast Brazil, *Tectonophysics*, *262*, 349–364.

Nicollet, C., and A. Leyreloup (1978), Petrologie des niveaux trondjhémitiques de haute pression associés aux éclogites et amphibolites des complexes leptyno amphiboliques du Massif Central Français, *Can. J. Earth Sci.*, *15*, 695–707.

Parrish, R. R. (1990), U-Pb dating of monazite and its application to geological problems, *Can. J. Earth. Sci.*, *27*, 1431–1450.

Petitpierre, E., and J.-L. Duthou (1980), Age westphalien par la methode Rb/Sr du leucogranite de Crevant, Plateau d'Aigurande (Massif Central Francais), *C. R. Acad. Sci.*, *291*, 163–166.

Pin, C., and D. Vielzeuf (1983), Granulites and related rocks in Variscan median Europe: A dualistic interpretation, *Tectonophysics*, *93*, 47–74.

Quenardel, J.-M., and P. Rolin (1984), Paleozoic evolution of the Plateau d'Aigurande (NE Massif Central, France), in *Variscan Tectonics of the North Atlantic Region*, edited by D. H. W. Hutton and D. J. Sanderson, *Geol. Soc. Spec. Publ.*, *14*, 47–61.

Roig, J.-Y., M. Faure, and P. Ledru (1996), Polyphase strike-slip tectonics in the southern French Massif Central: Kinematic inferences from pre- and syntectonic granitoids, *Geol. Rundsch.*, *85*, 138–153.

Rolin, P., and M. Colchen (2001), Carte structurale du socle Varisque Vendée-Seuil du Poitou-Limousin, *Geol. Fr.*, *1–2*, 3–6.

Rolin, P., and J.-M. Quenardel (1982), Modèle de mise en place syntectonique d'un massif de leucogranite hercynien (Crozant, NW du Massif Central Français), *C. R. Acad. Sci., Ser. II*, *294*, 463–466.

Rolin, P., J.-L. Duthou, and J.-M. Quenardel (1982), Datation Rb/Sr des leucogranites de Crozant et d'Orsennes: Conséquences sur l'âge de la dernière phase de tectonique tangentielle du Plateau d'Aigurande (NW du Massif Central Français), *C. R. Acad. Sci., Ser. II*, *294*, 799–802.

Sanderson, D. J., and W. R. D. Marchini (1984), Transpression, *J. Struct. Geol.*, *6*, 449–458.

Santallier, D., B. Briand, R.-P. Ménot, and M. Piboule (1988), Les complexes leptyno-amphiboliques (C. L. A.): Revue critique et suggestions pour un meilleur emploi de ce terme, *C. R. Acad. Sci.*, *8*, 3–12.

Santallier, D., J. M. Lardeaux, J. Marchand, and C. Marignac (1994), Metamorphism, in *Pre-Mesozoic Geology in France and Related Areas*, edited by J. D. Keppie, pp. 325–340, Springer, New York.

Scaillet, S., A. Cheilletz, M. Cuney, E. Farrar, and D. A. Archibald (1996a), Cooling pattern and mineralization history of the Saint Sylvestre and western Marche leucogranite pluton, French Massif Central: I. ^{40}Ar/^{39}Ar isotopic constraints, *Geochim. Cosmochim. Acta*, *60*, *23*, 4653–4671.

Scaillet, S., M. Cuney, C. Le Carlier de Veslud, A. Cheilletz, and J. J. Royer (1996b), Cooling pattern and mineralization history of the Saint Sylvestre and western Marche leucogranite pluton, French Massif Central: II. Thermal modelling and implications for the mechanisms of U-mineralization, *Geochim. Cosmochim. Acta*, *60*, 4673–4688.

Schmidt, N. H., and N. O. Olesen (1989), Computer-aided determination of crystal-lattice orientation from electron-channeling patterns in the SEM, *Can. Mineral.*, *27*, 15–22.

Schmitz, M. D., and S. A. Bowring (2001), U-Pb zircon and titanite systematics ofthe Fish Canyon Tuff: An assessment of high-precision U-Pb geochronology and itsapplication to young volcanic rocks, *Geochim. Cosmochim. Acta*, *65*, 2571–2587.

Schmitz, M. D., S. A. Bowring, K. R. Ludwig, and P. R. Renne (2003), Comment on ''Precise K-Ar, ^{40}Ar-^{39}Ar, Rb-Sr and U-Pb mineral ages from the 27.5 Ma FishCanyon Tuff reference standard'' by M. A. Lanphere and H. Baadsgaard, *Chem.Geol.*, *199*(3–4), 277–280.

Segall, P., and D. D. Pollard (1980), The mechanics of discontinuous faults, *J. Geophys. Res.*, *85*, 4337–4350.

Shaw, A. (1991), The petrogenesis of Hercynian granites, French Massif Central, Ph.D. thesis, Birkbeck College, Univ. of London, London.

Swanson, M. T. (1988), Pseudotachylyte-bearing strike-slip duplex structures in the Fort Foster Brittle Zone, S. Maine, *J. Struct. Geol.*, *10*, 813–828.

Sylvester, A. G. (1988), Strike-slip faults, *Geol. Soc. Am. Bull.*, *100*, 1666–1703.

Sylvester, A. G., and R. R. Smith (1976), Tectonic transpression and basement-controlled deformation in the San Andreas fault zone, Salton trough, California, *AAPG Bull.*, *60*, 74–96.

Tikoff, B., and M. de Saint Blanquat (1997), Transpressional shearing and strike-slip partitioning in the Late Cretaceous Sierra Nevada magmatic arc, California, *Tectonics*, *16*, 442–459.

Tikoff, B., and D. Greene (1997), Stretching lineations in transpressional shear zones: An example from the Sierra Nevada Batholith, California, *J. Struct. Geol.*, *19*, 29–39.

Tikoff, B., and C. Teyssier (1992), Crustal-scale, en échelon ''P-shear'' tensional bridges: A possible solution to the batholithic room problem, *Geology*, *20*, 927–930.

Tommasi, A., and A. Vauchez (1994), Magma-assisted strain localization in an orogen-parallel transcurrent shear zone of southern Brazil, *Tectonics*, *13*, 421–437.

Tullis, J., J. M. Christie, and D. T. Griggs (1973), Microstructures and preferred orientations of experimentally deformed quartzites, *Geol. Soc. Am. Bull.*, *84*, 297–314.

Turpin, L., M. Cuney, M. Friedrich, J.-L. Bouchez, and M. Aubertin (1990), Meta-igneous origin of Hercynian peraluminous granites in N. W. French Massif Central; implications for crustal history reconstructions, *Contrib. Mineral. Petrol.*, *104*, 163–172.

Valle Aguado, B., M. R. Azevedo, U. Schaltegger, J. R. Martinez Calalan, and J. Nolan (2005), U-Pb zircon and monazite geochronology of Variscan magmatism related to syn-convergence extension in Central Northern Portugal, *Lithos*, *82*, 169–184.

Van Den Driesche, J., and J. P. Brun (1989), Un modèle de l'extension paléozõuml;que supérieur dans le Sud du Massif Central, *C. R. Acad. Sci., Ser. II*, *309*, 1607–1613.

Van Den Driesche, J., and J.-P. Brun (1991), Tectonic evolution of the Montagne Noire (French Massif Central): A model of extensional gneiss dome, *Geodin. Acta*, *5*, 85–99.

Vanderhaeghe, O., and C. Teyssier (2001), Partial melting and flow of orogens, *Tectonophysics*, *342*, 451–472.

Vidal, P., J. Bernard-Griffiths, J.-J. Peucat, A. Cocherie, P. Lefort, and S. M. F. Sheppard (1984), Geochemical comparison between Himalayan and Hercynian leucogranites, *Phys. Earth Planet. Inter.*, *35*, 179–190.

Virlogeux, D., J. Roux, and D. Guillemot (1999), Apport de la géophysique à la connaissance du massif de Charroux-Civray et du socle poitevin, in *Etudes du massif de Charroux-Civray, Journées scientifiques CNRS/ANDRA, Poitiers, 13 et 14 octobre 1997*, pp. 33–62, EDP Sci., Les Ulis, France.

Vissers, R. L. M. (1992), Variscan extension in the Pyrenées, *Tectonics*, *11*, 1369–1384.

N. Arnaud, M. Brunel, and P. Monié, Laboratoire Dynamique de la Lithosphère, UMR 5573, Université Montpellier II, CC060, Place E. Bataillon, F-34095 cedex 5 Montpellier, France.

M. Faure, Institut des Sciences de la Terre d'Orléans, UMR 6113, Université d'Orléans, BP 6759, F-45067 Orléans cedex 2, France.

A. Gébelin, AREVA-BUM/DRH, 2 rue Paul Dautier BP 4, F-78141 Vélizy cedex, France. (aude.gebelin@wanadoo.fr)